UNCLASSIFIED

Prepared Under

Contract No. NASW-1408
National Aeronautic and Space Administration

A STUDY OF TIRES ON A WET RUNWAY
Final Report
Period Covered From
May 24, 1966 to September 24, 1967

RR 67-24   September, 1967

Prepared by   *A. Eshel*
 A. Eshel, Project Engineer

Approved by   *M. Wildmann*
 M. Wildmann, Manager
 Mechanics Section

AMPEX CORPORATION
RESEARCH AND ENGINEERING PUBLICATION

ACKNOWLEDGEMENT

ABSTRACT

In this work a foundation to the theory of hydroplaning is laid and solutions to simplified models are obtained. The report deals with the following aspects: hydrodynamics, tire elasticity and the coupling between them.

The hydrodynamic problem is broken into three regions: inlet, central and exit. Approximate equations for the central region including the effects of viscosity, fluid inertia and side flow are derived. Approximate boundary conditions for the inlet and exit are presented and a break-up into simpler subproblems is made.

Several tire elastic models of varying degrees of complexity are studied in view of the desire to couple them with the fluid flow.

Selected problems are numerically attacked and the results are graphically presented. A computer program for the evaluation of the pressure distribution and the load capacity for planar tires of arbitrary prescribed and fixed shape is available now. A program which in addition to that, takes in account a side flow estimate is also operating. A solution obtained for another model brings out qualitatively the effect of tire flexibility.

A number of other programs which take in account various models of flexibility as well as a more complete side flow treatment have also been developed. The results of some of the latter programs are not yet satisfactory and further work is needed for their completion.

CONTENTS

LIST OF FIGURES

NOMENCLATURE

A   Integration constant

b   Half-width of tire

B   Width parameter $= b/r_o$; Integration constant

C   Inertia parameter $= 1/2\ \rho U^2 / (p_t - p_a)$

D   Flexural rigidity of shell per unit width

f   Longitudinal velocity shape factor; perturbation from H

F   Integration constant

g   Lateral velocity shape factor

G   Integration constant; Green's function

h   Film thickness

$h_{1\infty}$ Separating streamline level at ∞

h_∞ Water level at ∞

h*   Film thickness where $f = 0$

h_o Level of reference-tire shape (Fig. 5.6.1; Fig. 3.1.1)

H   Dimensionless film thickness $= h/r_o$

H*   Dimensionless film thickness where $f = 0$

H_o Dimensionless level of reference $= h_o/r_o$

H_∞ Dimensionless water level at ∞

$H_{1\infty}$ Dimensionless height of separating streamline at ∞

K_D Dimensionless spring constant $D/[\,(p_t - p_a)\,r_o^2]$

K_T Dimensionless spring constant $T/[\,(p_t - p_a)\,r_o]$

K_W Dimensionless spring constant $kr_o/(p_t - p_a)$

k   Radial spring constant

L   Load parameter $= \text{Load}/[\,\text{width} \cdot (p_t - p_a)\,r_o]$

m   Root of characteristic equation

M_x Moment per unit width

M Moment parameter = Moment $/ \left[\text{width} \cdot (p_t - p_a) \cdot r_o^2 \right]$

P Reaction force at end of footprint

p Pressure under tire

p_t Inflation pressure

p_a Atmospheric pressure

Q Shear force per unit width

r_o Tire radius

R Local radius of curvature

T Tension per unit width

u x-velocity component

$\hat{u}$ Dimensionless x-velocity $= u/U$

U Tire velocity

v y-velocity component

w z-velocity component; radial deflection

w_o Tire deflection from reference state due to inflation

W Load

W_o Flexibility parameter $\dfrac{p_t - p_a}{k r_o}$

x Longitudinal coordinate

X Dimensionless longitudinal coordinate $\dfrac{x}{r_o}$

y Vertical coordinate

z Lateral coordinate

Z Dimensionless lateral coordinate $\dfrac{z}{r_o}$

β Angle of jet (Fig. 3.1.2)

δ Thickness of jet (Fig. 3.1.1); Deflection due to static loading (Fig. 5.6.2)

Δ Dimensionless thickness of jet $= \delta/r_o$; Dimensionless deflection due to static loading

ϵ	Viscosity parameter =	$\dfrac{6\mu U}{(p_t - p_a)\, r_o}$
θ	Slope of free surface	
χ	Normalized radius of curvature r_o/R	
μ	Viscosity	
π	Normalized pressure =	$\dfrac{(p - p_a)}{(p_t - p_a)}$
o	Density of water	
ζ	$= y/h$	
ξ	Dummy variable	

Subscripts

a	Atmospheric
c	Centerline
e	Exit
i	Inlet
∞	Undisturbed water
t	Tire

1.0 INTRODUCTION

1.1 Motivation

The braking capability of aircraft and other vehicles traveling on pneumatic tires has been known to be impaired by wet runway conditions. The phenomenon of tire skidding due to the formation of a liquid film under the tire has been termed hydroplaning.

1.2 Experiment Versus Theory

Important experimental work has been done on the problem by various researchers in this country and abroad. As a result of these efforts, some practical solutions to the problem have been proposed.

Efforts to develop a theory and to explain the underlying physical effects have, however, been quite limited. One reason for this is probably the very complex mathematical and physical nature of the problem. The purpose of the present work has been to attempt to bridge some of these gaps by developing a more adequate theory. The hope is that improved understanding of the mechanism of the phenomenon will help indicate the direction of improvement in the design of tires and roads.

1.3 Three Regions

In order to speak about the problem in more concrete terms, it may be helpful to picture three basic regions under the tire: inlet, central and exit regions (Fig. 1.3.1). The regimes of flow differ in these regions.
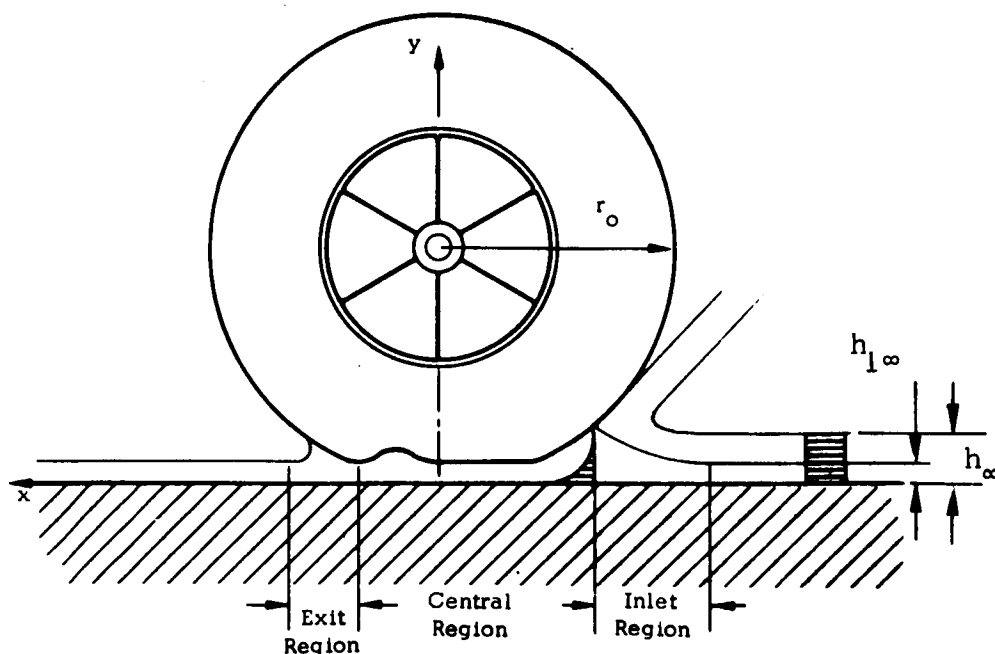
Fig. 1.3.1 Schematic View of Problem Under Consideration

The degree of complexity of this problem may be realized by considering the following features.

a.   Inertia effects are dominant in the inlet region.

b.   Viscous effects are important in the central region.

c.   Both the inlet and exit positions are not known apriori.

d.   The flexibility of the tire plays an important role in the phenomenon.

e.   A substantial fraction of the water encountered by the tire is deflected sideways.

f.   Additional features such as grooving, runway roughness, cavitation, and turbulence affect the problem.

The view has been taken at the beginning of the present work that the most promising avenue was to solve each region separately, thus taking advantage of whatever simplification its special character allowed. The separate solutions, however, have to be matched at their end points.

1.4 Method of Presentation

At first, it may seem logical to discuss the inlet, central, and exit regions – in this order. However, the fact is that the problem revolves around the central region to which the inlet and exit regions supply starting and end conditions. We shall start, therefore, with discussing the fluid mechanics of the central region, followed by discussions of the inlet and exit. Subsequently, we shall study the problem of tire elasticity and, finally, describe solutions to various models.

Several combinations of simplified models which are applicable, in varying degrees, to the problem at hand can be formulated. Our efforts were directed toward solving a number of these models. Solutions of some of the models have not been completed and need further work. Where deemed useful for future reference, these incomplete results are, nevertheless, presented in this report.

2.0 THE CENTRAL REGION

2.1   Derivation of an Integral Form of Navier-Stokes Equation and its
       Simplification

In this section the basic equations which are proposed and used in
this work for studying the central region are derived. Starting with the
Navier-Stokes equation in three dimensions, the derivation is based on
the following assumptions and restrictions:

a.   The pressure is uniform transverse to the film (vertically).

b.   The longitudinal and lateral velocity gradients are small
      compared to the transverse ones.

c.   The velocity profiles across the gap are assumed to be
      parabolic.

d.   The clearance does not vary laterally.

e.   The tire slides without rotation.

It is important to realize that these equations take into account both
viscous and inertia effects. Furthermore, the equations take into account
three dimensional flow. Due to the approximation made for the flow in the
vertical direction, the model will be termed, however, quasi three-dimensional.
The justification of assumptions (a) and (b) lies in the fact that the gap is
small. Assumption (c) is a first approximation, which could eventually be
improved by higher order polynominals. In section 2.4 we diverge from this
assumption. The restrictions (d) and (e) can be easily removed by generalizing
the derivation. We have chosen to impose these restrictions on the derivation
since it was clear at the outset that a great deal of work was needed before these
equations could be implemented in greater generality. For example, the

implementation of a laterally variable gap model hinges upon the use of three-dimensional tire models. Similarly, the consideration of the flow under a rotating tire requires corresponding elastic terms to be included.

With these approximations, the Navier-Stokes and the continuity equations in integral form may be written as follows:

$$\frac{\partial}{\partial x}\int_0^h \rho u^2 dy \;+\; \frac{\partial}{\partial z}\int_0^h \rho u w\, dy \;=\; -h\frac{\partial p}{\partial x} + \mu\int_0^h \frac{\partial^2 u}{\partial y^2} dy \qquad (2.1.1)$$

$$\frac{\partial}{\partial x}\int_0^h \rho u w\, dy \;+\; \frac{\partial}{\partial z}\int_0^h \rho w^2 dy \;=\; -h\frac{\partial p}{\partial z} + \mu\int_0^h \frac{\partial^2 w}{\partial y^2} dy \qquad (2.1.2)$$

$$\frac{\partial}{\partial x}\int_0^h \rho u\, dy \;+\; \frac{\partial}{\partial z}\int_0^h \rho w\, dy \;=\; 0 \qquad (2.1.3)$$

Assuming that the velocity profile is parabolic (Figs. 2.1.1 and 2.1.2),

$$\frac{u}{U} = (1-\zeta)(1+f\zeta) \qquad (u = 0 \text{ at } y = 0; \; u = U \text{ at } y = h) \qquad (2.1.4)$$

$$\frac{w}{U} = g\zeta(1-\zeta) \qquad (w = 0 \text{ at } y = 0 \text{ and at } y = h) \qquad (2.1.5)$$

where $\zeta = y/h(x)$, $g = g(x, z)$, and $f = f(x, z)$ are functions to be determined. The above integrals have the values

$$\int_0^1 \frac{u}{U} \, d\zeta = \frac{1}{2} + \frac{f}{6} \tag{2.1.6}$$

$$\int_0^1 \left(\frac{u}{U}\right)^2 d\zeta = \frac{1}{3} + \frac{f}{6} + \frac{f^2}{30} \tag{2.1.7}$$

$$\int_0^1 \left(\frac{w}{U}\right) d\zeta = \frac{g}{6} \tag{2.1.8}$$

$$\int_0^1 \left(\frac{w}{U}\right)^2 d\zeta = \frac{g^2}{30} \tag{2.1.9}$$

$$\int_0^1 \left(\frac{u}{U}\right)\left(\frac{w}{U}\right) d\zeta = \left(\frac{1}{12} + \frac{f}{30}\right) g \tag{2.1.10}$$

$$\int_0^1 \frac{\partial^2 (u/U)}{\partial \zeta^2} \, d\zeta = -2f \tag{2.1.11}$$

$$\int_0^1 \frac{\partial^2 (w/U)}{\partial \zeta^2} \, d\zeta = -2g \tag{2.1.12}$$

Substitution and simplification with the aim of obtaining expressions for

$$\frac{\partial f}{\partial x} \; , \; \frac{\partial f}{\partial z} \; , \; \frac{\partial g}{\partial x} \; , \; \frac{\partial g}{\partial z} \; , \; \frac{\partial p}{\partial x} \; , \; \frac{\partial p}{\partial z}$$

gives

$$\left(f + \frac{5}{2}\right)\frac{\partial f}{\partial x} + g\,\frac{\partial f}{\partial z} + \frac{3o}{\rho U^2}\frac{\partial p}{\partial x} = -\frac{6o\mu U}{\rho U^2 h^3}f + \frac{f-5}{2h}\frac{dh}{dx} \tag{2.1.13}$$

$$\left(f + \frac{5}{2}\right)\frac{\partial g}{\partial x} + g\,\frac{\partial g}{\partial z} + \frac{3o}{\rho U^2}\frac{\partial p}{\partial z} = -\frac{6o\mu U}{\rho U^2 h^3}g + \frac{g}{2h}\frac{dh}{dx} \tag{2.1.14}$$

$$\frac{\partial f}{\partial x} + \frac{\partial g}{\partial z} = -\frac{3+f}{h}\frac{dh}{dx} \tag{2.1.15}$$

We shall use the tire pressure as a parameter in nondimensionalizing the equations in view of future coupling of the fluid flow with the elasticity. The following dimensionless variables are introduced:

$$\Pi = \frac{p - p_a}{p_t - p_a} = C \cdot \frac{p - p_a}{\frac{1}{2}\rho U^2} \tag{2.1.16}$$

$$H = \frac{h}{r_o} \tag{2.1.17}$$
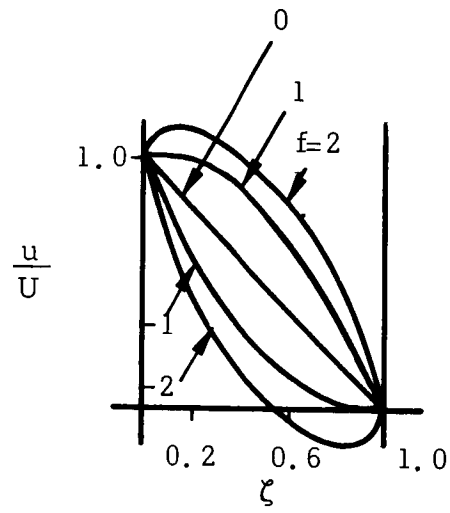
Fig. 2. 1. 1   The Longitudinal Velocity Profile .
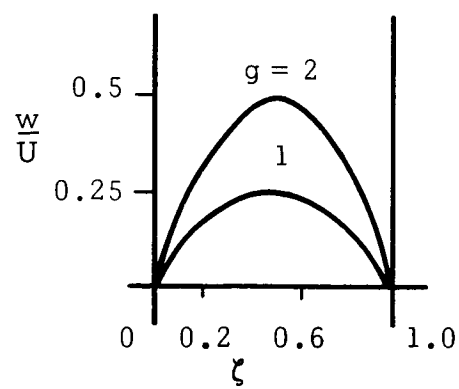
Fig. 2. 1. 2   The Lateral Velocity Profile

$$dX = \frac{dx}{r_0}$$

(2.1.18)

$$dZ = \frac{dz}{r_0}$$

(2.1.19)

$$\chi = \frac{r_0}{R}$$

(2.1.20)

and the dimensionless parameters used are:

$$\epsilon = \frac{6\mu U}{(p_t - p_a)r_0}$$ Viscosity parameter (2.1.21)

$$C = \frac{\frac{1}{2}\rho U^2}{p_t - p_a}$$ Inertia parameter (2.1.22)

$$B = \frac{b}{r_0}$$ Width parameter (2.1.23)

The formulation in terms of dimensionless variables becomes

$$\left(f + \frac{5}{2}\right)\frac{\partial f}{\partial x} + g\frac{\partial f}{\partial z} + \frac{15}{c}\frac{\partial \pi}{\partial x} = -\frac{5}{CH^2}f + \frac{f-5}{2H}\frac{dH}{dx}$$

(2.1.24),

$$\left(f + \frac{5}{2}\right)\frac{\partial g}{\partial x} + g\frac{\partial g}{\partial z} + \frac{15}{c}\frac{\partial \pi}{\partial z} = -\frac{5\epsilon}{CH^2}g + \frac{g}{2H}\frac{dH}{dx}$$

(2.1.25)

$$\frac{\partial f}{\partial x} + \frac{\partial g}{\partial z} = - \frac{3+f}{H} \frac{dH}{dx} \tag{2.1.26}$$

These equations form the basis for our treatment of the fluid mechanics in the central region. The y-coordinate has been eliminated from the equations through integration. It becomes clear now why we refer to these equations as only quasi three-dimensional.

2.2   Quasi Two-Dimensional Form of the Equations

In this section a particular form of Eqs. (2.1.13) to (2.1.15) is derived. In the particular case that variations in the z-direction are neglected (i.e., no side flow), the equations become:

$$\left(f + \frac{5}{2}\right) \frac{df}{dx} + \frac{30}{\rho U^2} \frac{dp}{dx} = - \frac{60 \mu U}{\rho U^2 h^2} + \frac{f-5}{2h} \frac{dh}{dx} \tag{2.2.1}$$

$$f = 3 \frac{p^*}{p} - 3 \tag{2.2.2}$$

or

$$\left(f + \frac{5}{2}\right) \frac{df}{dX} + \frac{15}{C} \frac{d\pi}{dX} = - \frac{5\epsilon}{C H^2} f + \frac{f-5}{2H} \frac{dH}{dX} \tag{2.2.3}$$

$$\frac{df}{dX} = -\frac{3+f}{H}\frac{dH}{dX} \qquad (2.2.4)$$

The continuity equation may be integrated once to give

$$f = 3\frac{H^*}{H} - 3 \qquad (2.2.5)$$

where H* is an integration constant which gives the value of H when f = 0, i. e. , when the velocity profile is linear (Fig. 2. 1. 1). Combining, we find

$$\frac{d\pi}{dX} = -\frac{\epsilon}{H^2}\left(\frac{H^*}{H}-1\right) + \frac{C}{15}\frac{dH}{dX}\left(\frac{9\,H^{*2}}{H^3} - \frac{4}{H}\right) \qquad (2.2.6)$$

The first term on the right-hand side is the viscous contribution. (Thus, when C = 0, the equation becomes the Reynolds equation of lubrication.) The second term on the right-hand side is the inertia term. Note that the sign of this term depends not only on the convergence or divergence of the passage (sign of dH/dX), but also on the sign of the parenthesized term (see Fig. 2. 2. 1).

2.3   Quasi Two-Dimensional Form of the Equations with Side Flow
        Estimate

As an intermediate step between the quasi two-dimensional model, which neglects any side flow, and the quasi three dimensional case, it is worthwhile considering a model where the flow is basically longitudinal, but a correction term involving an estimate of the side flow is used.

Let the side flow estimate be made on the basis of the following assumptions: First, the lateral inertia terms are neglected; and secondly, the lateral pressure distribution is assumed to be parabolic. Thus,

$$\frac{p - p_a}{p_t - p_a} = \frac{p_c - p_a}{p_t - p_a} \left[1 - \left(\frac{z}{b}\right)^2 \right]$$

(2.3.1)

where the subscripts a, t, and c denote atmospheric, tire, and centerline respectively. With these assumptions, Eqs. (2.1.13) to (2.1.15) become, respectively,
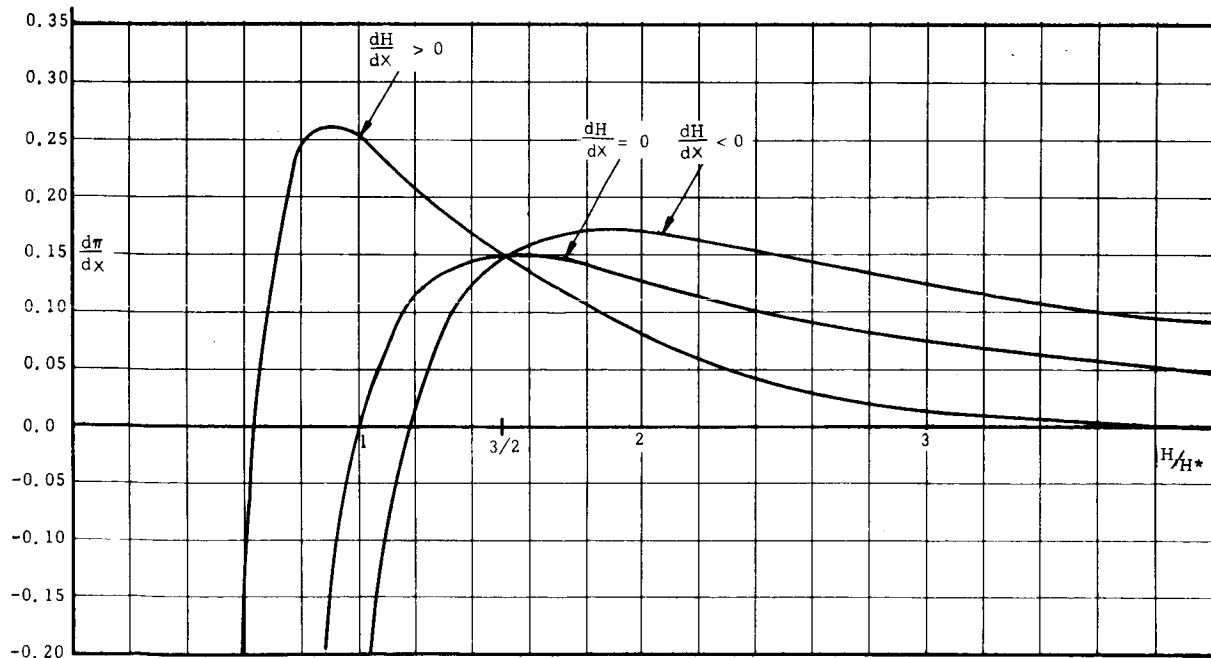
Fig. 2.2.1 Graphical Description of Eq. 2.2.6

$$\left(f + \frac{5}{2}\right)\frac{df}{dx} + \frac{30}{\rho U^2}\frac{dp_c}{dx} = -\frac{60\mu U}{\rho U^2 h^2}f + \frac{f-5}{2h}\frac{dh}{dx} \qquad (2.3.2)$$

$$q = 6\;\frac{p_c - p_a}{p_t - p_a}\;\frac{h^2}{br_o\left[\frac{6\mu U}{(p_t-p_a)r_o}\right]}\;\frac{z}{b} \qquad (2.3.3)$$

$$\frac{df}{dx} = -\frac{6}{r_o}\;\frac{p_c-p_a}{p_t-p_a}\;\frac{h^2}{b^2}\;\frac{1}{\dfrac{6\mu U}{(p_t-p_a)r_o}} + \frac{3+f}{h}\frac{dh}{dx} \qquad (2.3.4)$$

or alternatively,

$$\left(f + \frac{5}{2}\right)\frac{df}{dX} + \frac{15}{C}\frac{d\pi}{dX} = -\frac{5\epsilon}{CH^2}f + \frac{f-5}{2H}\frac{dH}{dX} \qquad (2.3.5)$$

$$q = 6\pi_c\left(\frac{r_o}{b}\right)^2\frac{H^2}{\epsilon}\,z \qquad (2.3.6)$$

$$\frac{df}{dX} = -6\pi_c H^2\left(\frac{r_o}{b}\right)^2\frac{1}{\epsilon} + \frac{3+f}{H}\frac{dH}{dX} \qquad (2.3.7)$$

2.4   Quasi Two Dimensional Non-Viscous Flow Formulation

The approach in this section is for special conditions different from the rest of the report. At a very high speed and small load, hydroplaning with large gaps may occur.   In this event the viscous forces are small, and the velocity profile may be nearly flat.   Under these circumstances the following equations may have validity in the central region:

$$u \cdot h = U \cdot h_{1\infty} \qquad \text{(Continuity)} \qquad (2.4.1)$$

$$\tfrac{1}{2} \rho u^2 + p = \tfrac{1}{2} \rho U^2 + p_a \qquad \text{(Bernoulli)} \qquad (2.4.2)$$

Here $h_{1\infty}$ is the level (at ∞) of the streamline separating the through flow which passes under the tire and the flow which is diverted.

In dimensionless form

$$\hat{u} \cdot H = H_{\infty} \qquad (2.4.3)$$

$$C + \pi = 1 \qquad (2.4.4)$$

3. 0 THE INLET REGION

3. 1   General Discussion and Prior Work

In the inlet flow pattern, the oncoming stream of water breaks into side flow, through flow and an upwards jet which may break into a spray.

If, to a first approximation, side flow and viscosity are neglected, the inlet flow model becomes that of a two-dimensional potential flow. Under these restrictions, the problems of an object gliding on the surface of a fluid of finite depth was analyzed by Green [1] in the 1930's for the special case of a flat plate (Fig. 3. 1. 1). This problem was further discussed by Gurevich [2] and Sedov [3]. The method of attack was the classical one of mapping the physical plane conformally onto the hodograph plane, a method particularly well suited for flows bounded by a combination of free surfaces and straight walls.

Martin [4] has obtained solutions for a number of special curved shaped (Fig. 3. 1. 2) by essentially analogous techniques with added degree of complexity due to the tire curvature.

We have studied Martin's work with the following objectives in mind:

(1)   Coupling Martin's solutions with our treatment of the central region.

(2)   Using Martin's work as a subroutine of an iterative procedure taking in account the flexibility in the following way: given a tire shape, find the pressure distribution then use the elastic model to find a more accurate tire shape.

After studying Martin's paper, we decided not to use his work at that stage, due to the following arguments. The complexity of these solutions is such that the deduction of additional necessary features for an already available solution, e. g. , the location of the stagnation point or the average pressure on a vertical plane through the stagnation point are laborious to obtain. Furthermore, this technique is not applicable directly to an arbitrary rigid tire shape but rather to special shapes only. Thus, in order to study the effect of tire flexibility by iteration, one has to use more elaborate means. For an arbitrary shape, the sought for mapping function is characterized by nonlinear integral side conditions. Some of the methods for setting such integral equations are discussed by Birkhoff and Zarantonello [5] and by Gurevich [2]. Finally, the use of conformal mapping is limited to two dimensions. Thus the theory cannot be readily extended into three dimensions.

3. 2 An Approximate Inlet Condition

Due to the complexity of Martin's technique and its limited applicability to coupling with the central region solution, we searched for simpler and more readily applicable techniques, even at some sacrifice in accuracy.

In the central region of the tire, viscous effects are important and parabolic velocity profile is assumed as explained in Chapter 2. 0. Thus, it becomes the function of the inlet region, to accommodate the uniform velocity profile prevailing upstream to the parabolic velocity profile prevailing in the central region. During this process of accommodation the inflow is diverted in part inot an upward jet and in part to side flow. Let the side flow in the inlet region be neglected to a first approximation. On this basis we shall derive in the following, using continuity and momentum balances on the control volume shown in Fig. 3. 1. 2, an accommodation condition. This relation can be used as an approximate initial condition for the central region. The continuity and momentum equations become:

$$h = -tg\ \beta \cdot x$$

Fig 3. 1. 1 Green's Problem – A Flat Plate Gliding over a Fluid
of Finite Depth

Control Volume

Fig 3. 1. 2 A Curved Plate Gliding over a Fluid of Finite Depth

$$0 = \int_0^{h_i} \rho u \, dy - \rho v h_\infty + \rho v \delta \tag{3.2.1}$$

$$(p_a - p_i) h_i = \int_0^{h_i} \rho u^2 \, dy - \rho v^2 h_\infty - \rho v^2 \delta \cos \beta_i \tag{3.2.2}$$

Using Eqs. (2.1.6) and (2.1.7), this becomes:

$$0 = \frac{1}{2} + \frac{f_i}{6} - \frac{h_\infty}{h_i} + \frac{\delta}{h_i} \tag{3.2.3}$$

$$-\pi_i = 2 C \left\{ \left[\frac{1}{3} + \frac{f_i}{6} + \frac{f_i^2}{30} \right] - \frac{h_\infty}{h_i} - \frac{\delta}{h_i} \cos \beta_i \right\} \tag{3.2.4}$$

For the evaluation of δ a mass balance between the reversed flow and the jet is made (See Fig. 2.1.1 for f < -1.)

$$0 = \int_{h_{i_1}}^{h_i} \rho u \, dy + \rho v \delta \tag{3.2.5}$$

where

$$\frac{h_{i_1}}{h_i} = - \frac{1}{f_i} \qquad \text{(Point of zero u)} \tag{3.2.6}$$

$$\frac{\delta}{R_i} = \frac{\Delta}{H_i} = -\left(\frac{1}{2} + \frac{f_i}{6} + \frac{1}{2f_i} + \frac{1}{6f_i^2}\right) \qquad (3.2.7)$$

where $\Delta = \dfrac{\delta}{r_o}$ is the dimensionless jet thickness.

Hence we find

$$\frac{H_\infty}{H_i} = -\frac{1}{2f_i} - \frac{1}{6f_i^2} \qquad (3.2.8)$$

$$\frac{\pi_i}{2c} = -\left(\frac{1}{3} + \frac{f_i}{6} + \frac{f_i^2}{30} + \frac{1}{2f_i} + \frac{1}{6f_i^2}\right) - \left(\frac{1}{2} + \frac{f_i}{6} + \frac{1}{2f_i} + \frac{1}{6f_i^2}\right) \cos\beta_i \qquad (3.2.9)$$

These two relations constitute initial conditions for the treatment of the central region. In order to facilitate their application, the relations are presented in graphical form in Figs. 3.2.1 and 3.2.2.

3.3 Comparison with Other Theories

In order to gain confidence in the initial conditions proposed in Section 3.2, a comparison with Green's solution [1] will be made here. Green solved the problem of a flat plate at angle of incidence β gliding over a fluid of finite depth (Fig 3.1.1).
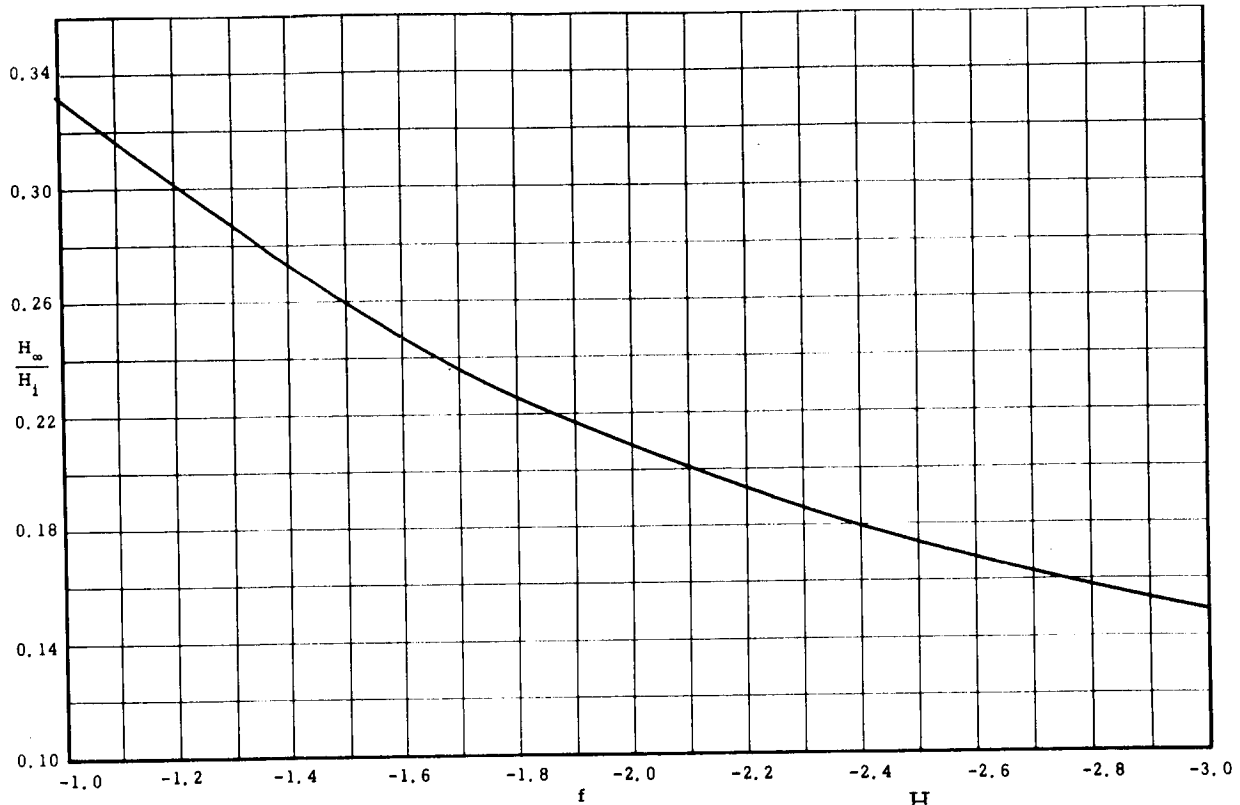
Fig. 3.2.1 Graphical Representation of the Function $\dfrac{H_\infty}{H_i} = \dfrac{1}{2f_i} - \dfrac{1}{6f_i^2}$
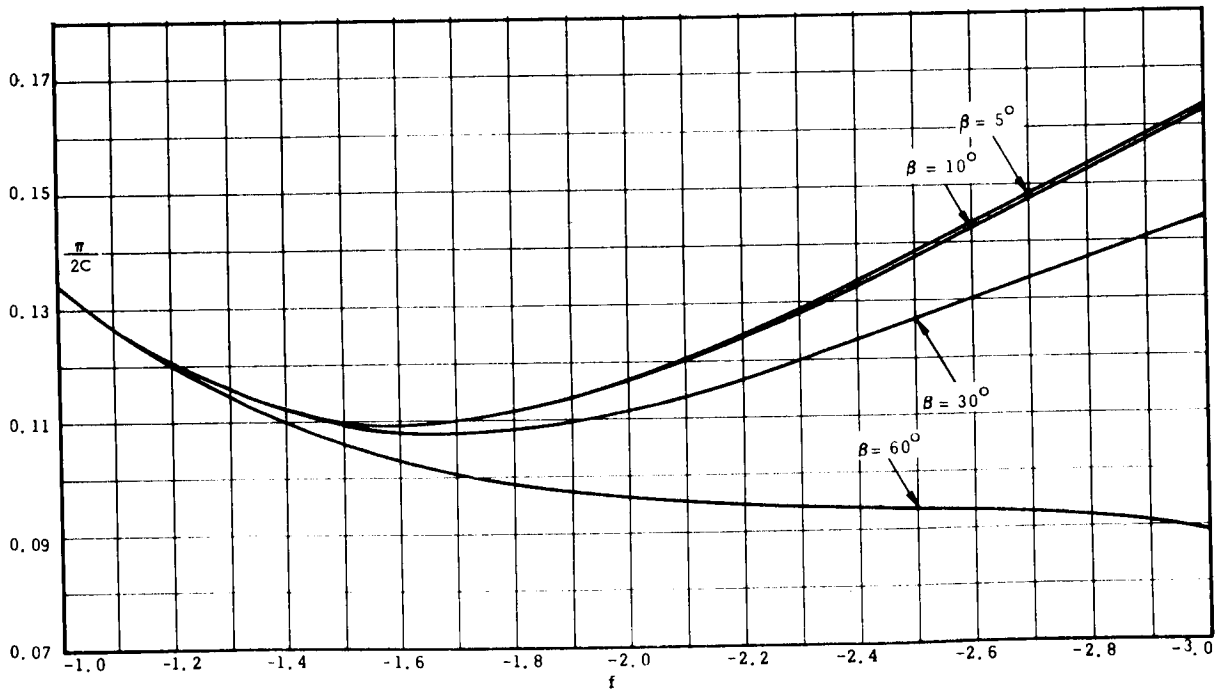
Fig. 3.2.2 Graphical Representation of the Function

$$\frac{\pi_i}{2C} = -\left(\frac{1}{3} + \frac{f_i}{6} + \frac{f_i^2}{30} + \frac{1}{2f_i} + \frac{1}{6f_i^2}\right) - \left(\frac{1}{2} + \frac{f_i}{6} + \frac{1}{2f_i} + \frac{1}{6f_i^2}\right) \cos \beta_i$$

Since Green considers non-viscous flow, it will be fair to assume $\mu = 0$ in Eq. (2.3.3) for the sake of comparison. Thus, we have *

$$\frac{d\pi}{dx} = -\frac{c}{15}\left(f + \frac{5}{2}\right)\frac{df}{dx} + \frac{c}{15}\frac{f-5}{2H}\frac{dH}{dx} \qquad (3.3.1)$$

$$f = 3\frac{H^*}{H} - 3 \qquad (3.3.2)$$

$$H = -tg\,\beta \cdot X \qquad (3.3.3)$$

Differentiating, we find

$$\frac{df}{dx} = \frac{3H^*}{tg\,\beta \cdot X^2} \qquad (3.3.4)$$

$$\frac{d\pi}{dx} = \frac{c}{15}\left(\frac{9{H^*}^2}{tg^2\beta\,X^3} - \frac{4}{x}\right) \qquad (3.3.5)$$

Using the boundary condition that the end of the plate is at $H = H_o$ and $\pi = 0$, we find

---

*h, h_o (Fig. 3.1.1), x are non-dimensionalized with respect to some characteristic length

$$\frac{\pi_i}{2c} = \frac{1}{30}\left[\frac{9}{2}\frac{H^{*2}}{H_i^2}\left(\frac{H_i^2}{H_o^2}-1\right) - 4\,ln\,\frac{H_i}{H_o}\right] \qquad (3.3.6)$$

$$\frac{\pi_i}{2c} = \frac{(f+3)^2}{60}\left(\frac{H_i^2}{H_o^2}-1\right) - \frac{2}{15}\,ln\,\frac{H_i}{H_o} \qquad (3.3.7)$$

In order to find the flow parameters we need a simultaneous solution of Eqs. (3.2.8), (3.2.9), (3.3.2) and (3.3.7). For H_i, π_i, f_i, H^*. In Fig. 3.3.1, the simultaneous solution of Eqs. (3.3.7) and (3.2.9) is shown. As explained before, this solution is motivated by the desire to compare the approximate conditions derived here to the available solution given by Green (Ref. [1], Fig. 8) who presents a chart which in our notation becomes:

$$\frac{H_o}{H_\infty} \qquad \text{versus} \qquad \frac{\delta}{h_\infty}\,c\,tg\,\frac{\beta_i}{2}$$

In Fig. 3.3.2 and 3.3.3 these variables are found as a function of f_i. Fig. 3.3.4 has been taken from Ref [1] and our results are superimposed. Our results become inaccurate for large values of H_o/H_∞. Consequently, we have not made the comparison for small angles β since the region of validity of our data is beyond the scale of Green's graphs. In most of the range of interest, our results compare well with those of Green. Our technique has, however, the advantage that it is mathematically simple, can accommodate viscous effects, is relatively easily coupled with the central region solutions, and can hopefully be generalized to three dimensions.
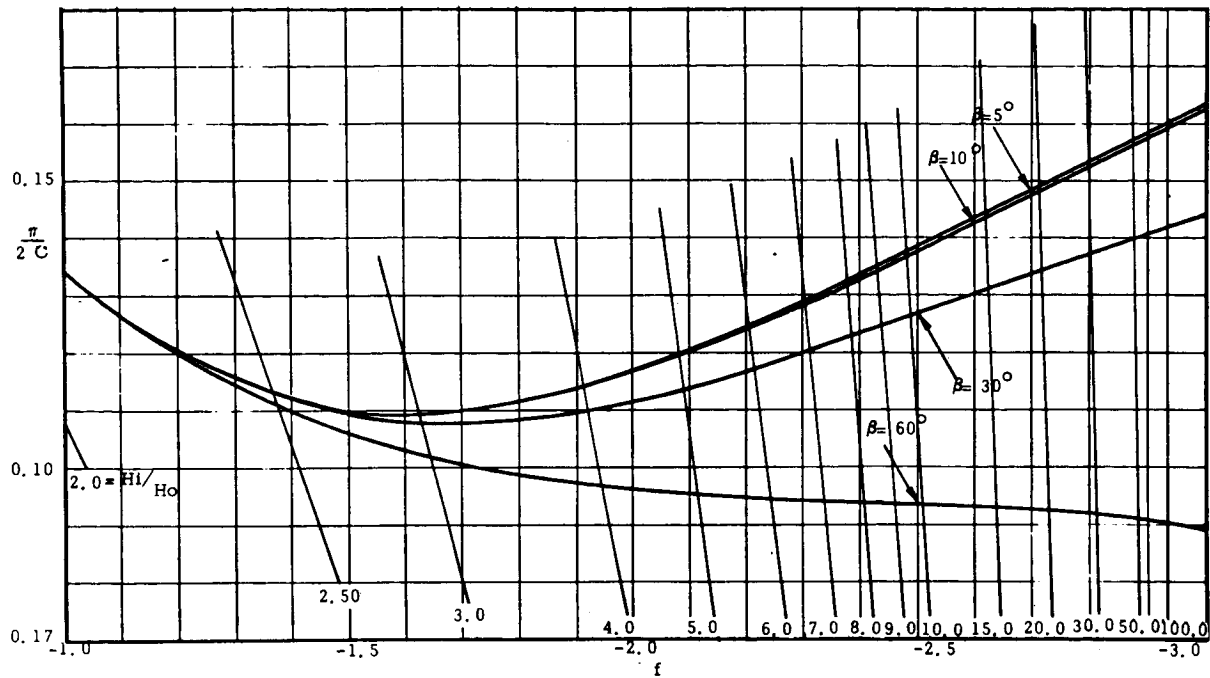
Fig. 3.3.1 Graphical Solution of the Equations

$$\frac{\pi_i}{2C} = \frac{(f+3)^2}{60}\left(\frac{H_i^2}{H_o^2}-1\right) - \frac{2}{15}\, ln\,\frac{H_i}{H_o} \quad and$$

$$\frac{\pi_i}{2C} = \left(\frac{1}{3}+\frac{f_i}{6}+\frac{f_i^2}{30}+\frac{1}{2f_i}+\frac{1}{6f_i^2}\right) - \left(\frac{1}{2}+\frac{f_i}{6}+\frac{1}{2f_i}+\frac{1}{6f_i^2}\right)\cos\beta_i$$
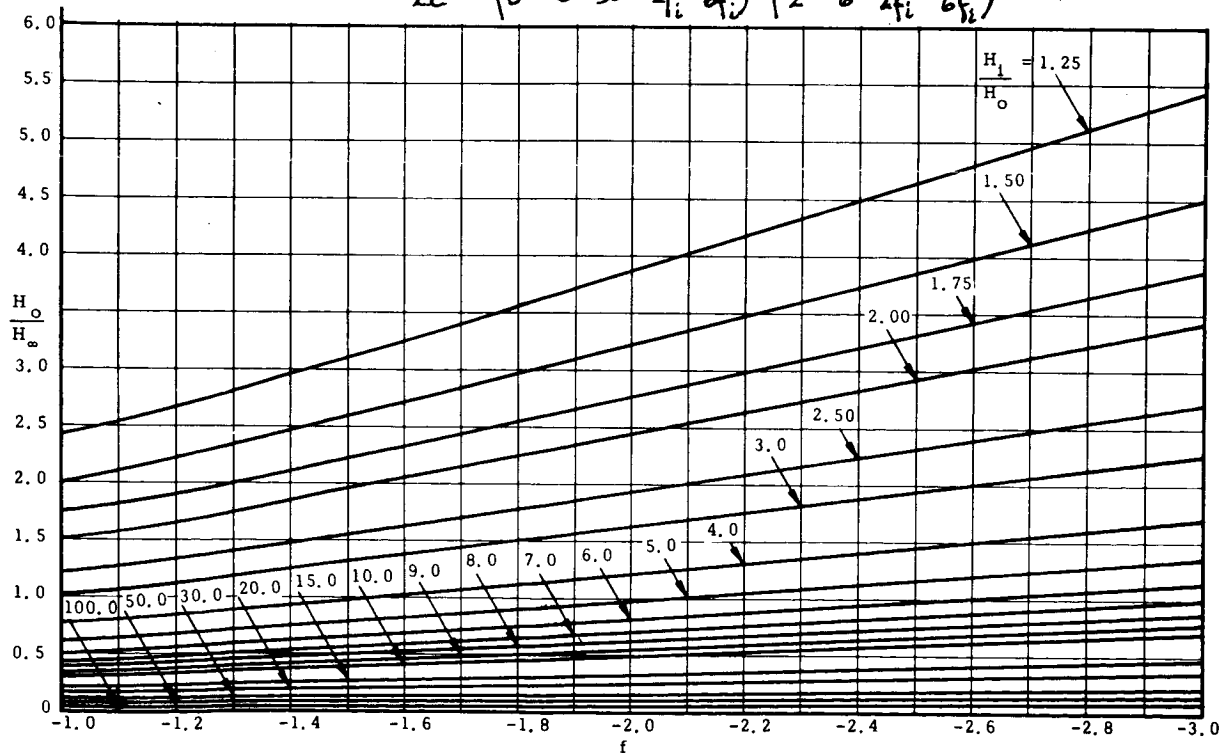
Fig. 3.3.2 Graphical Representation of $H_o/H_\infty = 1\Big/\left(\frac{H_\infty}{H_i}\cdot\frac{H_i}{H_o}\right)$

H_i/H_o is based on Fig. 3.3.1

H_∞/H_i is based on Fig. 3.2.2
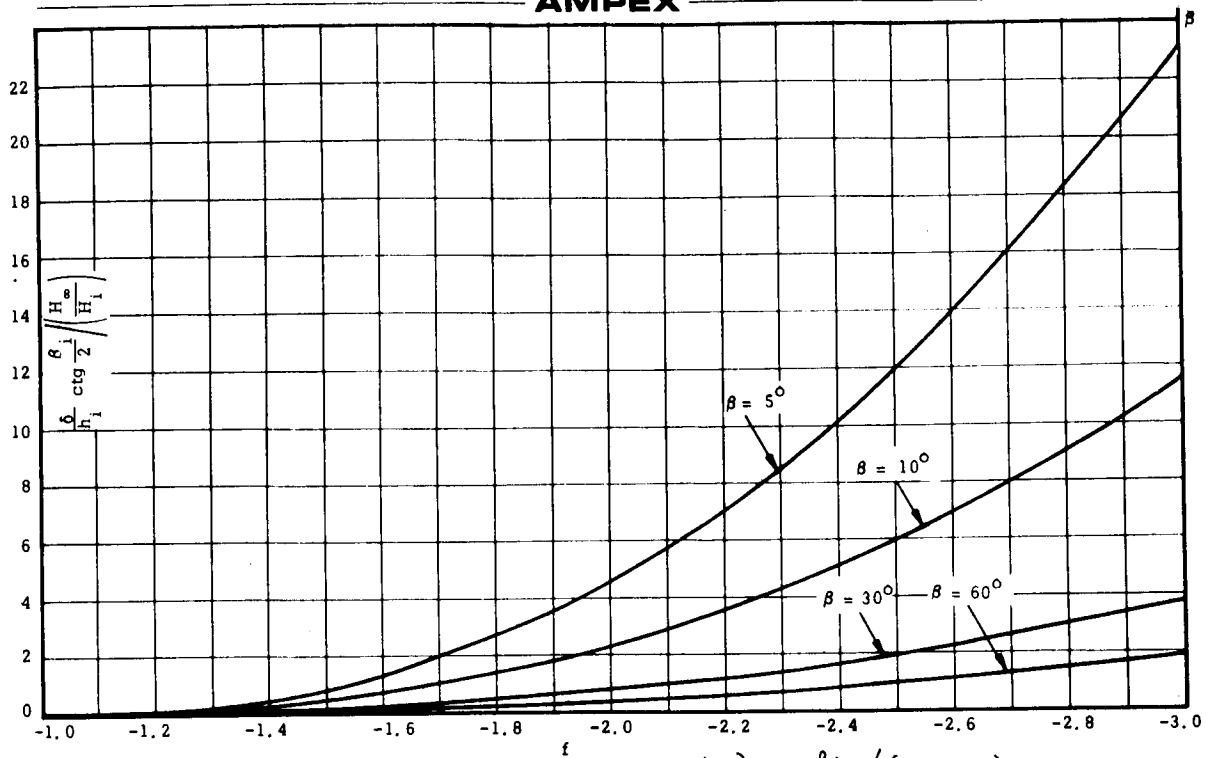
Fig. 3.3.3 Graphical Representation of $(\delta/h_i)\, ctg\, \frac{\beta_i}{2}\, /\, (H_\infty/H_i)$

δ/h_i is based on Eq. 3.2.7

H_∞/H_i is based on Fig. 3.2.2
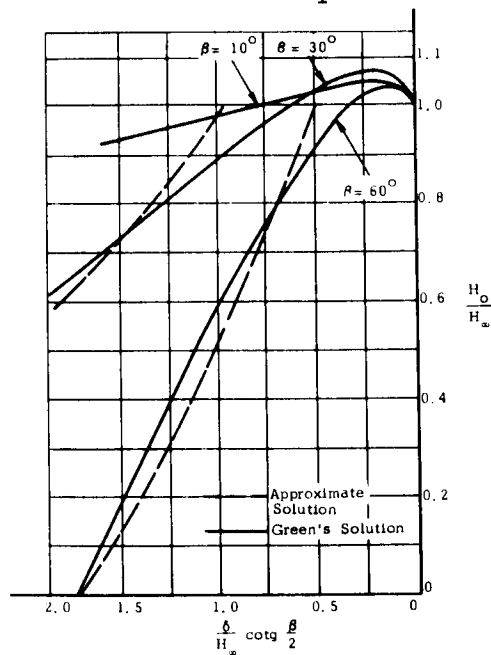
Fig. 3.3.4 Comparison of Fig. 8, Ref. [1], With the Approximate Solution Presented in this Work. Graphical Representation of

$$\frac{H_o}{H_\infty} \quad vs \quad \frac{(\delta/h_i)\, ctg\, \frac{\beta_i}{2}}{(H_\infty/H_i)}$$

4. 0   THE EXIT REGION

In order to solve the equations for the central region, conditions are needed not only for the inlet, but also for the exit. The question as to what exit conditions are applicable is not peculiar to the present work. This question arises in many lubrication problems and it is indeed difficult to answer it rigorously.

It has been a common practice in lubrication studies to assume that the film terminates where $\frac{dp}{dx} = 0$ and $p = p_a$. This is the swift-Stieber condition [6]. Another commonly used condition is to terminate the film at the point of incipient counterflow and $p = p_a$. This is the Birkhoff-Hays condition [7]. Both conditions have no rigorous rationalization. In heavily loaded bearings the choice of condition turns out not to affect significantly the prediction of load capacity. In a more rigorous investigation, Coyne and Elrod [8] derived exit pressure and exit pressure gradient conditions. Unfortunately, their investigation is limited to low Reynolds number. What is really needed here is to extend Coyne-Elrod's work into the higher Reynolds number range. From preliminary consideration we have concluded, however, that such an extension is a problem which requires a special program of study. In order not to embark on work beyond the scope of the present project, we have tentatively applied the Birkhoff-Hays exit condition to our solutions.

5. 0 TIRE FLEXIBILITY

5. 1   Introduction

A most important aspect of hydroplaning is the effect of tire flexibility. Perhaps the most striking example of the importance of flexibility is the NASA formula [9] which asserts that the speed of incipient hydroplaning is proportional to the square root of the tire pressure. Thus, the greater the flexibility, the higher is the hydroplaning danger. Secondly, films on hydroplaning [10] reveal inward bulging of the tire in its footprint area. This cannot occur if flexibility is neglected. As a final example, it has been noted by Gross, Stahler and Wildmann [11] that the pressure distribution in foil bearings [12] * whose essential characteristic is high flexibility, is remarkably similar to that measured under tires (see Fig. 5. 1. 1).

A number of tire structural models are studied in this chapter. We start in Section 5. 2 with a brief review of some of the literature on the subject. Following this, we summarize in Section 5. 3 some of the common aspects of many models. In Sections 5. 4 through 5. 8, we present detailed analyses of each of the models we considered. These models are arranged, with one exception, in increasing order of complexity. Accordingly, Section 5. 8 should have preceded Section 5. 7. We diverted from this order since the basic equations of Section 5. 8 can be deduced directly from those of Section 5. 7 by putting $D = 0$.

---

*The foil bearing concept is described in more detail in Section 5. 5.
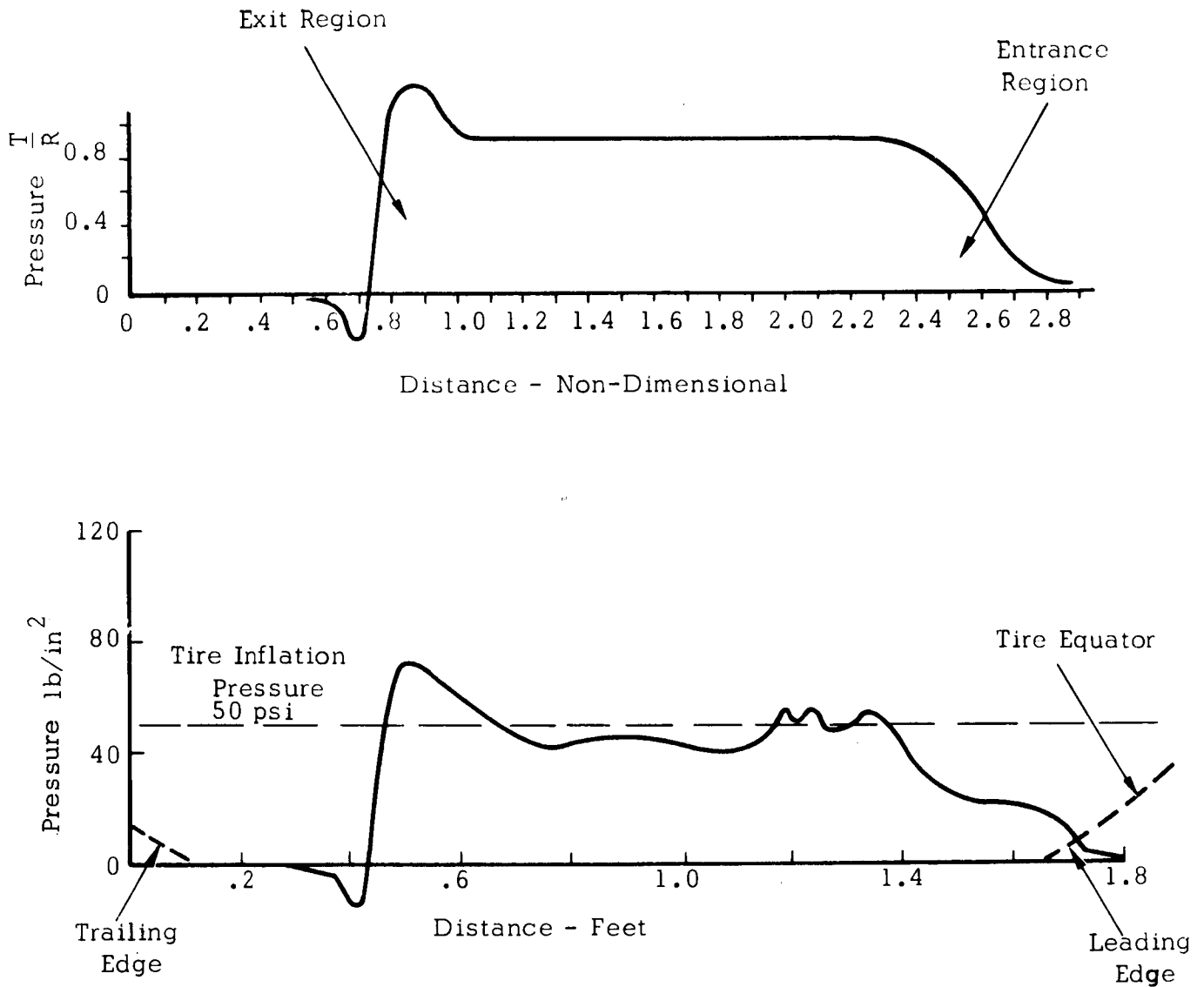
Fig. 5.1.1 Calculated Pressure Distribution Under a Perfectly
Flexible, Self-Acting Foil Bearing (adapted from
Ref. 12) and Measured Pressure Distribution Under
a Tire (adapted from Reference 27)

5.2   Literature on Tire Elastic Models

There exists no elastic model of tires which is both satisfactory
and simple. The main complicating factors are:

1.   The geometry of the tire which constitutes a pre-stressed
     toroidal shell of non-circular cross section.

2.   Tire materials are non-linear and exhibit viscoeleastic
     behavior.

3.   Due to the structural reinforcement the elastic properties
     of the composite tire material are non-isotropic.

Some of the analytical studies of the elastic structure of tires are
outlined below. Ames and Lauterbach [13, 14] applied the theories of
Adkins, Rivlin and Hofferberth [15 through 20] to formulate a membrane
model in which the load was considered to be supported by the network of
cords with a negligible contribution of the rubber. A further development [21],
which takes in account the laminated structure shows how to calculate the
deformations due to an axisymmetric load. Another approach was taken by Clark
[22], who considered the tire as an elastically supported cylindrical shell.

Bergman [23] was interested in cornering forces. He considered the
tire as composed of a large number of rings, each sliced by two neighboring
planes intersecting on the axis of rotation. These rings were considered as lateral
springs. More involved models were used by Saito [24], Lippmann [25] and
others who treated the tread region as a beam supported on the sidewalls which
were considered as an elastic foundation.

5.3   General Remarks about Treatment of Flexibility

In principle, one can find the pressure distribution for a given tire
shape from considerations of <u>fluid mechanics</u>.   The equations involved in
this were discussed in Chapters 2.0 to 4.0. Any structural tire model
relates a local load distribution through <u>elastic</u> and <u>geometric</u> conditions
to a clearance distribution. The present chapter is devoted to this problem.

One general method of simultaneously evaluating the pressure
and the clearance distribution is solving each of these problems separately
and _iterating_. The other alternative is _coupling_ the equations by eliminating
the pressure. The iterative approach is available for use with any tire model.
It involves usually convergence problems which have to be overcome. The
coupling approach produces for all but the simplest tire models high-order
differential equations. The solution of high order boundary value problems
is usually difficult due to the growth of spurious solutions in the integration
process.

Another one of the problems encountered in this work was the
evaluation of tire elastic parameters. The approach used to resolve this
problem was to deduce load-deflection-footprint curves for the theoretical
models and to fit them to experimental data*. This task has been accomplished
for the spring and membrane models. It has not been completed yet for the
shell model although the formulae are all presented in Section 5.7.

It is convenient to define load and moment parameters to be used
later.

$$L = \frac{Load/Width}{(p_t - p_a) r_o} = \frac{\int_{x_i}^{x_e} (p - p_a) dx}{(p_t - p_a) r_o} = \int_{x_i}^{x_e} \pi \, dx \tag{5.3.1}$$

$$M = \frac{Moment/Width}{(p_t - p_a) r_o^2} = \frac{\int_{x_i}^{x_e} (p - p_a)(x - r_o \frac{dh}{dx}) dx}{(p_t - p_a) r_o^2} = \int_{x_i}^{x_e} \pi (x - \frac{dH}{dx}) dx \tag{5.3.2}$$

---

*The experimental data used in this chapter has been provided by the
Goodyear Tire and Rubber Company.

Here x_i and x_e denote, respectively, the inlet and exit points or the attachment and detachment points of the film.

Whether in loading against a dry flat plate or on a fluid film, changes of some degree of abruptness in the loading occur at some points. It is therefore important to investigate the conditions of continuity in H and its derivatives. These conditions will be derived in the following sections separately for each model.

5.4   Rigid Tire

When the technique of iteration is used to account for the flexibility effects it will be found necessary to assume an initial rigid tire shape. A circular shape is probably the most natural first approximation. Since the region of interest is the footprint, the approximation of

$$\frac{d^2 h}{dx^2} \cong \frac{1}{R} \tag{5.4.1}$$

has been utilized in this work. Accordingly, a circular tire of radius of curvature $R = r_o$, will give in the region of interest a gap distribution of

$$h = a + bx + \frac{x^2}{2r_o} \tag{5.4.2}$$

If one chooses the origin as the intersection point between the axis of symmetry of the tire and the ground, this relation becomes

$$h = h_o + \frac{x^2}{2r_o} \tag{5.4.3}$$

where h_o is the height of the minimum point of the tire contour. In dimension-less form:

$$H = H_o + \frac{X^2}{2}$$

(5. 4. 4)

5. 5 Foil Bearing Model

The term "foil bearing" was coined in 1953 by Blok and Van Rossum [26] in reference to a bearing surface made of a flexible foil stretched between distant supports. Interest at Ampex in foil bearings stems from the fact that the configuration of a tape gransported over guiding spindles or magnetic recording heads is a foil bearing. As the flexible tape passes over the spindle it entrains an air film. This is similar to the water film formed between the compliant tire surface and the road. In some applications, interest is to promote air lubrication while in other instances the requirement is to destroy the film. The latter case is analogous to the tire problem.

Mathematically, the planar foil bearing used as a tire model involves the simultaneous solution of a flow equation and the elasticity relation

$$p_t - p = \frac{T}{R}$$

(5. 5. 1)

with the proper boundary conditions. Here p, p_t, R, T denote the local and the tire pressures, radius of curvature and tension respectively. The clearance h and the local radius of curvature R are related through geometry (Eq. 5. 4. 1). The tension T may be estimated as

$$T = (p_b - p_a) r_o \qquad\qquad (5.5.2)$$

In dimensionless form Eq. (5.5.1) becomes

$$1 - \pi = \frac{d'^2 H}{dx^2} \qquad\qquad (5.5.3)$$

The pressure distribution in foil bearings and tires is remarkably similar (Fig. 5.1.1). Nevertheless, the problems are significantly different in the following respects:

1. The flow model in the classical foil bearing solutions is based on the Reynolds Equation and involves no inertia effects. These effects are important in the tire case and particularly in the inlet.

2. The elastic structure of the tire is much more complex than that of a perfectly flexible tape.

3. The most significant difference in character between tires and foils lies, however, in the fact that foil bearings do not transmit hub loads while tires are loaded through the hub.

Only in the event that a section of a tire transmits little hub load, can it be expected that a simulation by means of a foil will have some measure of success. The center plane of a wide tire fulfills to a limited extent this condition. This plan is far from the side walls of the tire. If one neglects the loads transmitted by lateral tension and by the radial shear, this plane is affected by a force balance resembling that of a foil bearing (Fig. 5.5.1).

Section of Circumferential Wall
Which Resembles a Foil
Bearing

z - Tension on Membrane

Relatively Stiff Side Wall

Hub

P_t

p
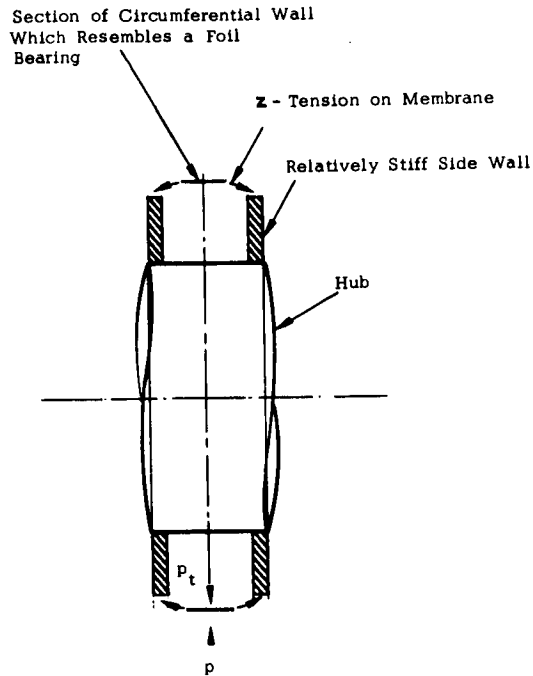
Fig. 5. 5. 1   The Foil Bearing as a Tire Model

5. 6   Spring Model

The foil bearing has a basic deficiency as a tire model in that
it cannot transmit hub loads.   The simplest model which does not exhibit
this difficulty is composed of a continuous distribution of radial springs.
These springs can be thought of as simulating both the stiffness of the
side walls and the hoop stiffness of the circumference.   If the springs are
assumed to be independent circumferentially but tied laterally (planar deflection),
the equations describing pressure deflection relation is

$$p_t - p = k w \tag{5.6.1}$$

Here k is the spring constant in units of pressure change per unit deflection. The local delfection measured outward from the stress free state is denoted by w. The dimensionless deflection is $W = w/r_o$.

In dimensionless form Eq. (5. 6. 1) becomes

$$1 - \pi = W/W_o \tag{5. 6. 2}$$

where

$$W_o = \frac{p_t - p_a}{k \cdot r_o} \tag{5. 6. 3}$$

W_o may be interpreted as a dimensionless deflection due to inflation. The reciprocal $K_W = 1/W_o$ may be interpreted as a dimensionless spring constant.

In addition to this elastic equation, a geometric condition relating the deflection w to the clearance h is needed. Figure 5. 6. 1 defines the quantities θ, h_o, x. When the angle θ is small, this geometric relation may be approximated by

$$h + w = h_o + \frac{x^2}{2 r_o} \tag{5. 6. 4}$$

or

$$H + W = H_o + \frac{x^2}{2} \tag{5. 6. 5}$$

The spring model as an approximation to a real tire in the sense of Fig. (5. 5. 1) applies particularly to the region close to the side walls.

Continuity Conditions

It is clear from Eq. (5. 6. 1) that a discontinuous pressure distribution will cause discontinuous tire contour and point forces cannot be accommodated at all.

Static Load on Dry Surface

The load deflection-footprint relation will be derived here for the purpose of fitting the stiffness parameters by comparison to experimental data. Denote the inward deflection (measured from the inflated tire shape) that the tire undergoes due to loading against a flat plate, by δ. Thus, it is seen from Fig. 5. 6. 2 that

$$\delta = w_o - h_o \tag{5.6.6}$$

$$\Delta = \frac{\delta}{r_o} = W_o - H_o = \frac{1}{K_w} - H_o \tag{5.6.7}$$

At the end of the footprint X_e:

$$\pi_e = 0$$

so that

$$W_e = W_o.$$

Contour of Tire with no
Load and no Pressure
Applied

Contout of Actual
Loaded Tire
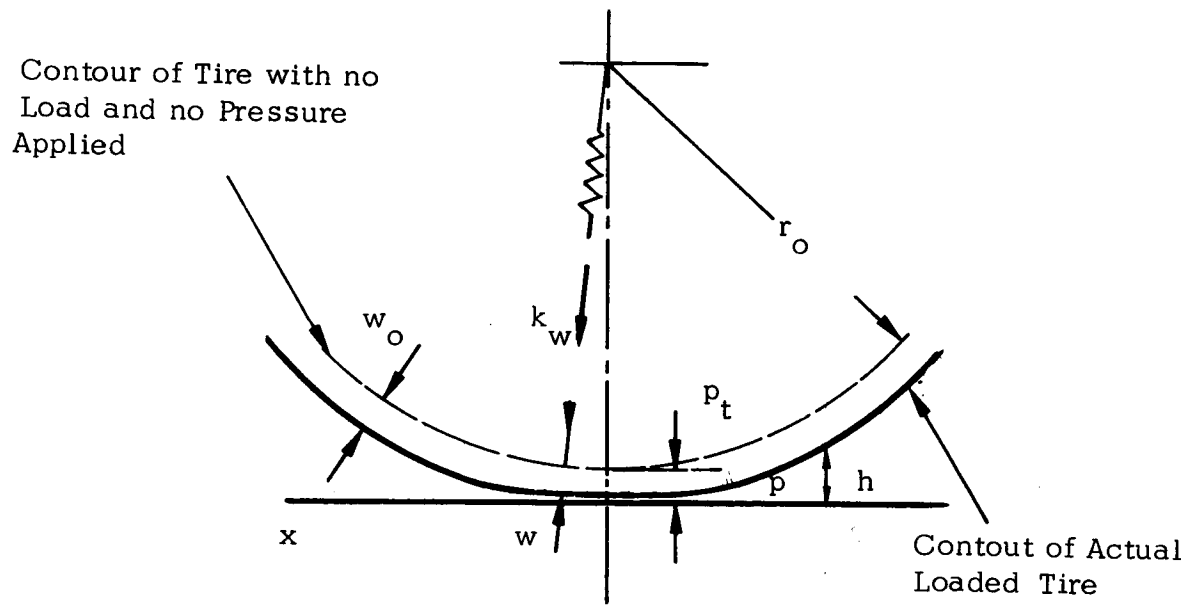
Fig. 5. 6. 1 Notation for the Tire Spring Model
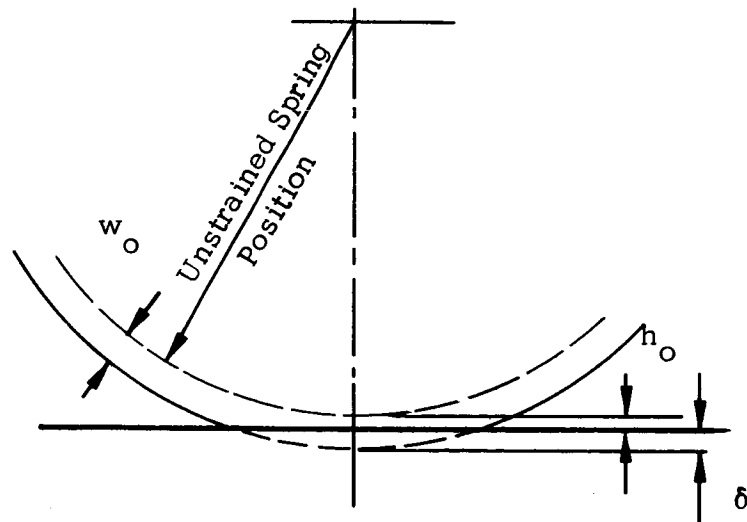
Fig. 5. 6. 2 Notation for Static Loading

Furthermore, at the end of the footprint

$$H_e = 0$$

It follows from Eq. (5.6.5) that

$$\Delta = W_o - H_o = X_e^2 / 2 \qquad (5.6.8)$$

The pressure distribution in the footprint follows from Eqs. (5.6.2) and (5.6.5).

$$\pi = 1 - K_w W = 1 - K_w \left(H_o + \frac{x^2}{2} \right) \qquad (5.6.9)$$

The load parameter is

$$L = 2 \int_0^{X_e} \pi \, dX = 2 \left(1 - K_w H_o \right) X_e - \frac{K_w X_e^3}{3} \qquad (5.6.10)$$

or

$$L = 1.89 \, K_w \, \Delta^{3/2} = \frac{2}{3} \, K_w \, X_e^3 \qquad (5.6.11)$$

On the basis of these formulae, curve-fitting to the Goodyear data has been made and the results are shown in Fig. 5. 6. 3.

5.7 Elastically supported Laterally Rigid Shell (Tire Shell Model)

Let us consider a __planar__ model consisting of a cylindrical shell supported on continuous radial springs (playing the role of the side walls) and pressurized to a pressure p_t. This is similar to the model considered by Clark [22].

The force and moment balances on an element as well as the stress strain relations become (Fig. 5.7.1)

$$p_t - p - kw - T\frac{d^2h}{dx^2} - \frac{dQ}{dx} = 0 \tag{5.7.1}$$

$$Q = \frac{dM_x}{dx} \tag{5.7.2}$$

$$M_x = D\left(\frac{1}{r_o} - \frac{d^2h}{dx^2}\right) \tag{5.7.3}$$

where k is the spring constant (pressure change per unit deflection), T the tension per unit width and D the flexural rigidity per unit width. w is the outward deflection measured from the zero spring-strain position. In deriving these equations it was assumed that the surface under consideration is flat enough that

$$1 \gg \left(\frac{dh}{dx}\right)^2 \qquad \text{i.e.,} \qquad \frac{1}{R} \cong \frac{d^2h}{dx^2}$$

41
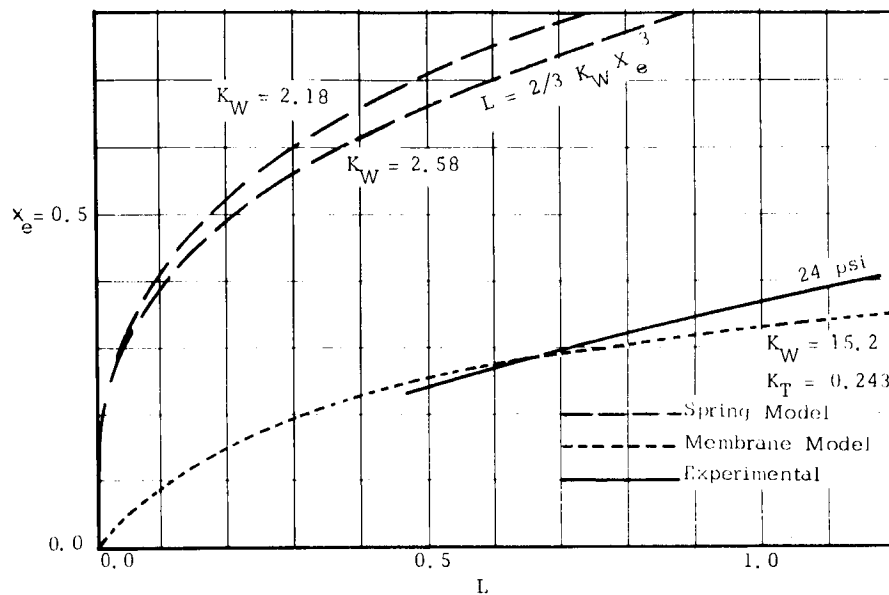
Fig. 5. 6. 3 Experimental and Theoretical Load-Deflection Curves
(The experimental curves, courtesy of Goodyear Tire and
Rubber Company - 8. 25 x 14 Power Cushion)
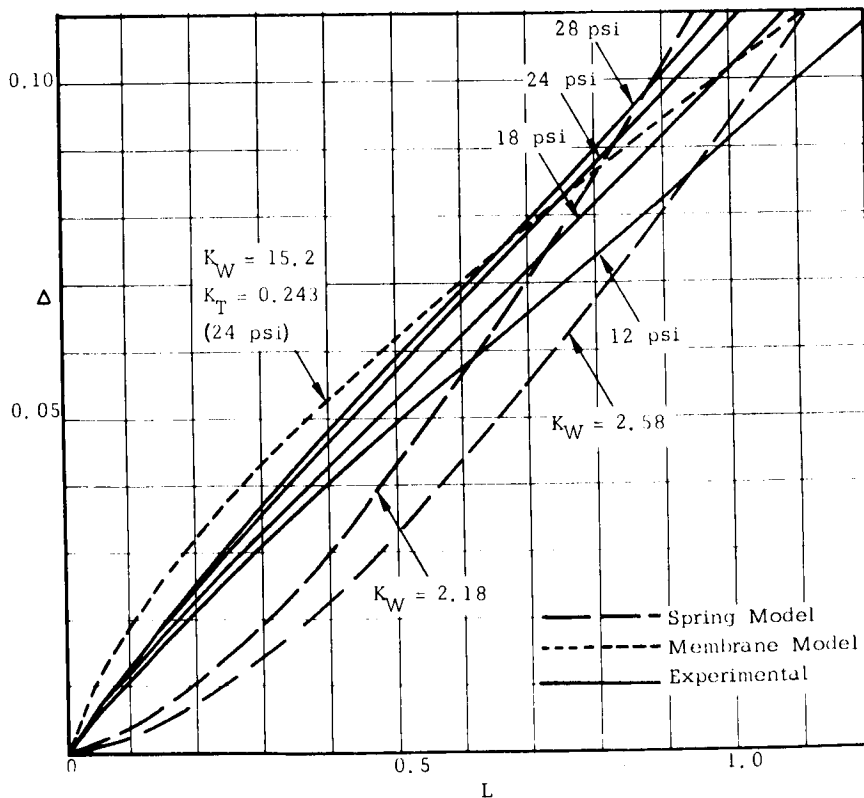
Fig. 5. 6. 4 Experimental and Theoretical Load-Footprint Curves
(The experimental curve, courtesy of Goodyear Tire and
Rubber Company - 8. 25 x 14 Power Cushion)

and that the tangential load as well as the circumferential tension variations are neglibible. Thus:

$$p_t - p = -D \frac{d^4 h}{dx^4} + T \frac{d^2 h}{dx^2} + kw \tag{5.7.4}$$

$$h + w = h_o + \frac{x^2}{2r_o} \tag{5.7.5}$$

or

$$D \frac{d^4 h}{dx^4} - T \frac{d^2 h}{dx^2} + kh = k \left(h_o + \frac{x^2}{2r_o} \right) - (p_t - p) \tag{5.7.6}$$
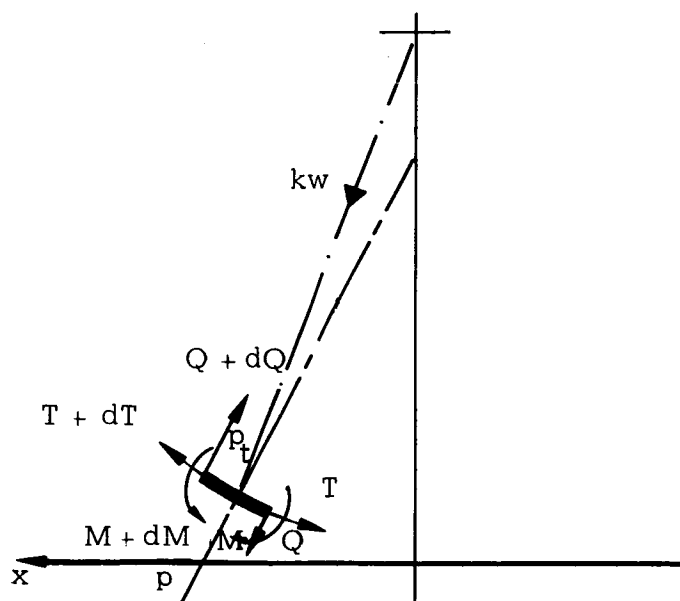
Fig. 5.7.1   Notation for the Tire-Shell and Membrane Models

A prescribed h_o determines the position of the tire center and thus determines the load.

The tension T is assumed in this treatment to be uniform around the tire for a given tire pressure regardless of the hub load. Thus, for a given inflation pressure, the tension may be regarded as a prescribed elastic constant. In dimensionless form, Eq. (5.7.6) becomes:

$$K_D \frac{d^4 H}{dx^4} - K_T \frac{d^2 H}{dx^2} + K_W H = K_W \left(H_o + \frac{x^2}{2} \right) + \pi - 1 \qquad (5.7.7)$$

where

$$K_D = \frac{D}{(p_t - p_a) r_o^3} \qquad (5.7.8)$$

$$K_T = \frac{T}{(p_t - p_a) r_o} \qquad (5.7.9)$$

$$K_W = \frac{k r_o}{p_t - p_a} \qquad (5.7.10)$$

Deflection Due to Inflation

Let us assume that due to inflation the tire deflects from the unstrained spring state an amount w. Thus the tension T can be found in terms of w from Eq. 5.7.4

$$p_b - p_a = \frac{T}{r_o} + k w_o$$

(5.7.11)

$$1 = K_T + K_W W_o$$

(5.7.12)

In the spring model, $K_T = 0$. There we found that $W_o = 1/K_W$

Continuity Conditions

It is important, as explained before, to determine up to what order of differentiation, continuity of the derivatives of H is maintained in face of discontinuities in load.

From Eq. (5.7.2) it is clear that the moment M_x must be continuous if we exclude infinite point loads. Therefore, it is seen from Eq. (5.7.3) that H" must also be continuous.

Let us consider now an interval of width 2ε around a point X on which we fix our attention. Integration of Eq. (5.7.7) across this interval gives

$$\Delta H''' = H'''(X+\varepsilon) - H'''(X-\varepsilon) =$$

(5.7.13)

$$= \frac{1}{K_D} \int_{X-\varepsilon}^{X+\varepsilon} \left[K_T \frac{d^2 H}{dX^2} - K_W H + K_W \left(H_o + \frac{X^2}{2} \right) + 1 \right] dX + \frac{1}{K_D} \int_{X-\varepsilon}^{X+\varepsilon} \pi dX$$

45

The first integral on the right hand side vanishes when $\varepsilon \to 0$. It is concluded, therefore, that a jump in H''' occurs whenever a point force is applied, i.e., when the second integral remains finite as $\epsilon \to 0$. A finite discontinuity in pressure may cause, however, a discontinuity in the H^{IV} but not in H'''

Static Load on Dry Surface

We will continue to use here the notation of Fig. 5.6.2.

$$\delta = w_o - h_o \tag{5.7.14}$$

or in dimensionless form

$$\Delta = W_o - H_o = \frac{1 - K_T}{K_W} - H_o \tag{5.7.15}$$

The solution of Eq. (5.7.7) for the region which is not in contact $(\pi = 0)$ is

$$H = A e^{m_1 X} + B e^{m_2 X} + F e^{-m_1 X} + G e^{-m_2 X} + H_o + \frac{X^2}{2} - \frac{1 - K_T}{K_W} \tag{5.7.16}$$

where

$$m_{1,2} = \sqrt{\frac{K_T \pm \sqrt{K_T^2 - 4 K_D K_W}}{2 K_D}}$$

RR 67-24

are the solutions of the characteristic equation of the homogeneous part of Eq. (5.7.7). In the footprint area the solution is

$$H = 0 \tag{5.7.17}$$

and hence the pressure distribution becomes

$$\pi = 1 - K_w \left(H_o + x^2/2 \right) \tag{5.7.18}$$

This, however, is not the complete solution since it will be shown soon that supplementary point forces are applied at the edges of the footprint. The solution for $X > X_e \geq 0$ where X_e is one end of the footprint, involves four integration constants. Two of these constants, A, B must vanish in order that H will not blow up exponentially as $X \to \infty$. The remaining two constants must be determined by the continuity conditions at X_e.

It is now seen that unless one assumes that an upward point force P is applied at X_e, four continuity requirements are imposed with only two degrees of freedom F, G left for evaluation. We thus come up with the conclusion that at X_e a finite jump in the third derivative occurs. The continuity requirements are:

$$H = 0 = F e^{-m_1 X_e} + G e^{-m_2 X_e} + \frac{X_e^2}{2} - \Delta \tag{5.7.19}$$

$$H' = 0 = -m_1 F e^{-m_1 X_e} - m_2 G e^{-m_2 X_e} + X_e \tag{5.7.20}$$

$$H'' = 0 = m_1^2 F e^{-m_1 X_e} + m_2^2 G e^{-m_2 X_e} + 1 \qquad (5.7.21)$$

$$\Delta H''' = \frac{P r_o^2}{D} = -m_1^3 F e^{-m_1 X_e} - m_2^3 G e^{-m_2 X_e} \qquad (5.7.22)$$

With X_e prescribed, Eqs. (5.7.19) to (5.7.20) can be used to evaluate the unknown F, G, Δ, P:

$$G = \frac{1 + m_1 X_e}{m_2 (m_1 - m_2)} e^{m_2 X_e} \qquad (5.7.23) *$$

$$F = \frac{1 + m_2 X_e}{m_1 (m_2 - m_1)} e^{m_1 X_e} \qquad (5.7.24)$$

$$\Delta = \frac{1 + (m_2 + m_1) X_e}{m_1 m_2} + \frac{X_e^2}{2} \qquad (5.7.25)$$

$$\frac{P r_o^2}{D} = m_1 + m_2 + m_1 m_2 X_e \qquad (5.7.26)$$

---

*It will be shown later that Eqs. (5.7.23 to 5.7.27) are applicable only for $\Delta > \dfrac{1}{m_1 m_2}$.

The load can be evaluated at the point by means of Eq. (5.2.18).

$$Load/Width = 2(p_t - p_a)r_o \int_0^{X_e} \pi\, dx + 2P$$

$$= 2(p_t - p_a)r_o\left[(1 - K_w H_o)X_e - \frac{K_w X_e^3}{6}\right] + \frac{2D}{r_o^2}\left[m_1 + m_2 + m_1 m_2 X_e\right]$$

(5.2.27)

At this point it is natural to inquire what happens to Δ when $X_e \to 0$. At a first thought, one is tempted to say that Δ should approach zero. Eq. (5.7.25) reveals at once that this is not the case. The reason for this behavior lies in the fact that Eqs. (5.7.19) through (5.7.21) stem from the applicability of Eq. (5.7.17) in the footprint. When $X_e \to 0$, the footprint vanishes and while Eq. (5.7.20) is still right by virtue of symmetry, Eq. (5.7.21) does not apply. In fact the ground reaction is a point force and the curvature at the single point of contact is somewhere between zero and $1/r_o$ depending on the load. We have found, therefore, that this model exhibits two types of behavior as one increases the load from zero*. For small but finite loads, the tire ground contact is at a single point ($X_e = 0$) where a point reaction force acts. As the load increases from zero to some threshold value, the radius of curvature at the contact point increases from r_o to ∞ and the footprint forms. Further increase in load will increase X_e from zero and generate a ground pressure along the footprint in addition to point forces at its ends.

In the low load range the equivalent to Eqs. (5.6.19) to (5.7.22) is

---

*It should be noted that this is the behavior of our model and not necessarily of real tires. At the point of application of a point force an unrealizable infinite pressure occurs. In reality a distribution of pressure and local surface deformations exist. Local deformations of this nature are neglected in our model and in thin shell theory in general. The overall effects are nevertheless correct, by virtue of St. Venant's principle.

$$H = 0 = F + G - \Delta \tag{5.7.28}$$

$$H' = 0 = -m_1 F - m_2 G \tag{5.7.29}$$

$$H'' = \chi = m_1^2 F + m_2^2 G + 1 \tag{5.7.30}$$

$$\Delta H''' = \frac{Pr_0^2}{D} = -m_1^3 F - m_2^3 G \tag{5.7.31}$$

These equations are applicable for a given Δ in the range

$$0 \leq \Delta \leq \frac{1}{m_1 m_2} \tag{5.7.32}$$

for solving F, G, P, χ

The solution is

$$F = \frac{m_2 \Delta}{m_2 - m_1} \tag{5.7.33}$$

$$G = \frac{m_1 \Delta}{m_1 - m_2} \tag{5.7.34}$$

$$\chi = 1 - m_1 m_2 \Delta \tag{5.7.35}$$

$$\frac{Pr_0^2}{D} = m_2 m_1 \left(m_1 + m_2 \right) \Delta \tag{5.7.36}$$

The load for the range

$$0 \leq \Delta \leq \frac{1}{m_1 m_2}$$

is:

$$\text{Load/width} = 2P = \frac{D}{r_o^2} m_1 m_2 (m_1 + m_2) \Delta \qquad (5.7.37)$$

The purpose of the derivation of these load-deflection-footprint relations was to make it possible to evaluate the coefficients K_D, K_T, K_W from experimental data. This task has not been completed.

General Solution of Eq. (5.7.7) for a Prescribed Pressure Distribution

The purpose of the following derivation is to find an expression or an algorithm for the evaluation of H once π is known. This will be useful as a part of an iterative-coupling of the fluid flow to the tire shell model. Substituting the expression

$$H = H_o + \frac{K_T - 1}{K_W} + \frac{x^2}{2} + f \qquad (5.7.38)$$

in Eq. (5.7.7), the equation becomes:

$$K_D f^{\overline{iv}} - K_T f'' + K_W f = \pi \qquad (5.7.39)$$

51

where we require $f \to 0$, for $x \to \pm \infty$.

Let us find the Green's function $G(x, \xi)$ for the problem. This function is defined by the differential equation

$$K_D G^{\overline{IV}} - K_T G'' + K_W G = 0 \qquad (5.7.40)$$

and the following boundary and continuity conditions:

$$\lim_{x \to \pm \infty} G = 0 \qquad (5.7.41)$$

At

$$x = \xi$$

$$G, \quad G', \quad G'' \qquad \text{are continuous and}$$

$$G'''(\xi^+) - G'''(\xi^-) = \frac{1}{K_D} \qquad (5.7.42)$$

The function G is found to be as follows

$$G(x,\xi) = -\frac{e^{m_1(x-\xi)}}{2K_D m_1\left(m_2^2-m_1^2\right)} + \frac{e^{m_2(x-\xi)}}{2K_D m_2\left(m_2^2-m_1^2\right)} \qquad -\infty < x < \xi \qquad (5.7.43)$$

$$G(x,\xi) = -\frac{e^{-m_1(x-\xi)}}{2K_D m_1\left(m_2^2-m_1^2\right)} + \frac{e^{-m_2(x-\xi)}}{2K_D m_2\left(m_2^2-m_1^2\right)} \qquad \xi < x < \infty$$

Accordingly,

$$f(x) = \int_{-\infty}^{\infty} \pi(\xi)\, G(x,\xi)\, d\xi \tag{5.7.44}$$

or since $\qquad \pi(x) \equiv 0 \qquad$ for $\qquad x < x_i \; ; \; x_e < x$

$$H(x) = H_o + \frac{x^2}{2} + \frac{K_T - 1}{K_w} + \int_{x_i}^{x_e} \pi(\xi)\, G(x,\xi)\, d\xi \tag{5.7.45}$$

When $\pi(X)$ is found from fluid mechanical considerations, $H(X)$ can, in principle, be evaluated from Eq. (5.7.45).

5.8   Elastically Supported, Laterally Rigid Membrane (Tire – Membrane Model)

The model discussed in this section is simpler than the tire-shell model. It follows the tire-shell model in the sequence of presentation merely due to the fact that by putting D=0 in Eq. (5.7.6) the basic equations is found.

This model can be visualized as a cylindrical shell with infinite lateral bending stiffness and perfect flexibility in the longitudinal direction. This shell is elastically supported in the radial direction. This is in a way a combination of the foil bearing model and the spring model. The basic equation is:

$$T \frac{d^2 h}{dx^2} - k h = p_t - p - k \left(h_o + \frac{x^2}{2r_o} \right) \qquad (5.8.1)$$

or in dimensionless form

$$K_T \frac{d^2 H}{dx^2} - K_W H = 1 - \pi - K_W \left(H_o + \frac{x^2}{2} \right) \qquad (5.8.2)$$

where again

$$K_T = \frac{T}{(p_t - p_a) r_o} \qquad (5.8.3)$$

$$K_W = \frac{k r_o}{p_t - p_a} \qquad (5.8.4)$$

Continuity Conditions

     The motivation for deriving these conditions has been given before and will not be repeated here. From Eq. (5.8.2) it is clear that a pressure jump along the periphery of the tire requires H" to be discontinuous. Integrating this equation across a jump of width 2 ϵ where $\epsilon \to 0$ shows that

$$\Delta H' = H'(x + \epsilon) - H'(x - \epsilon) = \frac{1}{K_T} \int_{x-\epsilon}^{x+\epsilon} \left(1 + K_W H - K_W \left(H_o + \frac{x^2}{2} \right) \right) dx - \int_{x-\epsilon}^{x+\epsilon} \pi \, dx \qquad (5.8.5)$$

Hence, if H is continuous, $\Delta H'$ vanishes unless $\int_{X-\varepsilon}^{X+\varepsilon} \pi dx$ is finite, i.e., only if a point force is applied, a discontinuity in H' will exist.

Boundary Conditions

The boundary condition for H' at the inlet and the exit points in the case of fluid flow under the tire may be established by solving Eq. 5.8.2 for the case of $\pi = 0$. This condition exists in the regions $\infty > x > x_e$; $x_i > x > -\infty$. The general solution is

$$H = A e^{-\sqrt{\frac{K_W}{K_T}}X} + B e^{\sqrt{\frac{K_W}{K_T}}X} + H_o + \frac{X^2}{2} + \frac{K_T-1}{K_W} \qquad (5.8.6)$$

For the exit region B = 0, hence

$$H' = -A\sqrt{\frac{K_W}{K_T}} e^{-\sqrt{\frac{K_W}{K_T}}X} + X \qquad (5.8.7)$$

$$H'_e = -\sqrt{\frac{K_W}{K_T}} \left(H_e - H_o - \frac{X_e^2}{2} - \frac{K_T-1}{K_W}\right) + X_e \qquad (5.8.8)$$

For the inlet:

$$H'_i = \sqrt{\frac{K_W}{K_T}} \left(H_i - H_o - \frac{X_i^2}{2} - \frac{K_T-1}{K_W}\right) + X_i \qquad (5.8.9)$$

Static Load on Dry Surface

Consider now the problem of a tire statically loaded on a dry surface. The expression (5.7.15) for the static deflection Δ applies here too. In the footprint area

$$H = 0 \qquad (5.8.10)$$

Hence, the application of the continuity requirements mentioned above, at the boundaries at the footprint (i) and (e) gives:

$$H_e = H_i = 0 \quad ; \quad H_e' = H_i' = 0 \qquad (5.8.11)$$

The size of the footprint is found by substitution of Eq. (5.8.11) into Eq. (5.8.8).

$$X_e^2 + 2\sqrt{\frac{K_T}{K_W}} X_e + 2H_o + 2\frac{K_T - 1}{K_W} = 0 \qquad (5.8.12)$$

$$X_e = -X_i = -\sqrt{\frac{K_T}{K_W}} + \sqrt{\frac{2 - K_T}{K_W} - 2H_o} \qquad (5.8.13)$$

56

The pressure distribution in the footprint due to dry loading is found by substituting Eq. (5.8.10) into Eq. (5.8.2)

$$\Pi = 1 - K_W \left(H_o + \frac{x^2}{2} \right) \tag{5.8.14}$$

The load parameter is:

$$L = \int_{X_i}^{X_e} \left[1 - K_W \left(H_o + \frac{x^2}{2} \right) \right] dx \tag{5.8.15}$$

$$L = \left(2 - 2 K_W H_o \right) x_e - \frac{K_W x_e^3}{3} \tag{5.8.16}$$

where X_e is given by Eq. (5.8.13). The set of equations (5.8.13), (5.8.16) and the expression

$$\Delta = W_o - H_o = \frac{1 - K_T}{K_W} - H_o = \frac{x_e^2}{2} + \sqrt{\frac{K_T}{K_W}} x_e \tag{5.8.17}$$

have been used to evaluate the coefficients K_W and K_T on the basis of the Goodyear data (Fig. 5.6.3).

6. 0 FORMULATIONS AND SOLUTIONS

6. 1   Introduction

In this chapter formulations and solutions for specific models will be presented. In addition, some of our work which still requires further efforts for completion, is described.

6. 2   Quasi Two Dimensional Flow Model Coupled with a Rigid Circular Tire*

Equations   (See Section 2. 2; 5. 4)

$$\frac{d\pi}{dx} = -\frac{\epsilon}{H^2}\left(\frac{H^*}{H}-1\right) + \frac{C}{15}\frac{dH}{dx}\left(\frac{9H^{*2}}{H^3} - \frac{4}{H}\right) \tag{6.2.1}$$

$$f = 3\frac{H^*}{H} - 3 \tag{6.2.2}$$

$$H = H_o + \frac{x^2}{2} \tag{6.2.3}$$

Input Parameters

ϵ, C, H*, H_o

_____

* Note that the prescribed shape was arbitrarily chosen to be circular. The technique applies to any shape.

Boundary Conditions (integration in the negative direction).

At the exit:

$$\pi_e = 0$$

$$f_e = -1 \quad \text{(Section 4.0)}$$

(H_e and X_e are found from Eqs. (6.2.2) and (6.2.3)).

The numerical integration of Eq. (6.2.1) supplies a relation between π and H. The attachment point (π_i, H_i) must belong to this family. At the inlet: Eq. (3.2.0) supplies a second relation between π_i and H_i so that the inlet point is determined.

Output Parameters

H_∞ (from Eq. (3.2.8)), Δ (from Eq. 3.2.7) and L (from Eq. (5.3.1).

This is an inverse solution of the problem. We prescribe the flow rate (H*) and the tire center level by specifying H_o and find as output the values of the water level (H_∞), the jet thickness Δ, and the load (L). This technique eliminates trial and error.

Results

In Fig. 6.2.1 to 6.2.3 sample pressure distributions are shown. The effects of speed are demonstrated by varying simultaneously C and ϵ in the following way: $C \sim U^2$; $\epsilon \sim U$. Increase in speed results in higher pressure level and in a deeper penetration of the inlet region into the footprint area Secondly, the effect of prescribing the flow rate is studied by specifying H*. The variations of load and pressure due to small changes in flow rate are rather strong.

Fig. 6.2.1
Pressure Distribution in Quasi
Two-Dimensional Flow Under
Rigid Circular Tire
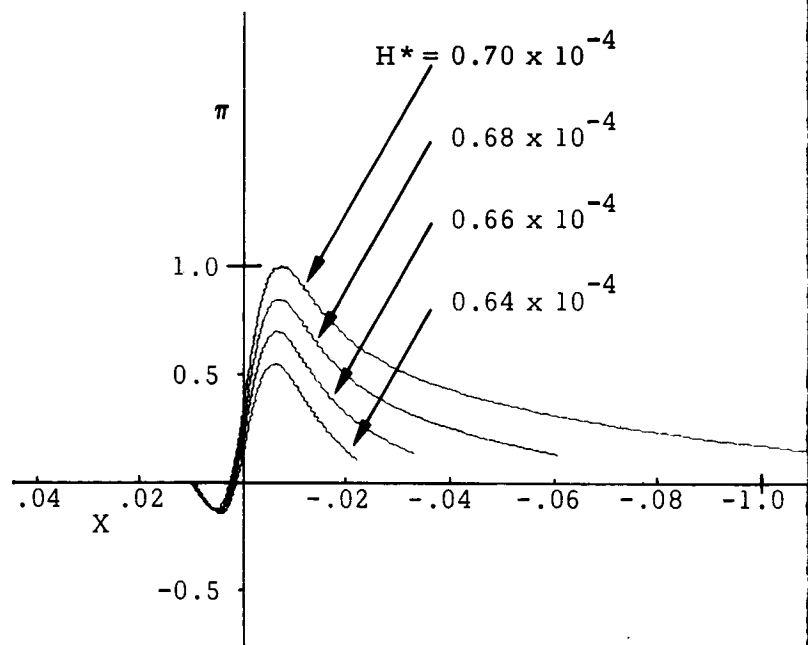
H*	L	H_∞	Δ
0.070×10^{-3}	0.0451	0.9442×10^{-3}	0.9092×1
0.068×10^{-3}	0.0237	0.2894×10^{-3}	0.2554×1
0.066×10^{-3}	0.0125	0.0980×10^{-3}	0.0650×1
0.064×10^{-3}	0.0069	0.0529×10^{-3}	0.0209×1

$H_O = 0.5 \times 10^{-4}$

$C = 0.5$

$\epsilon = 10^{-6}$

H*
0.070×10
0.068×10
0.066×10
0.064×10

$$H^* = 0.70 \times 10^{-4}$$
$$0.68 \times 10^{-4}$$
$$0.66 \times 10^{-4}$$
$$0.64 \times 10^{-4}$$

$$H^* = 0.70 \times 10^{-4}$$
$$0.68 \times 10^{-4}$$
$$0.66 \times 10^{-4}$$
$$0.64 \times 10^{-4}$$
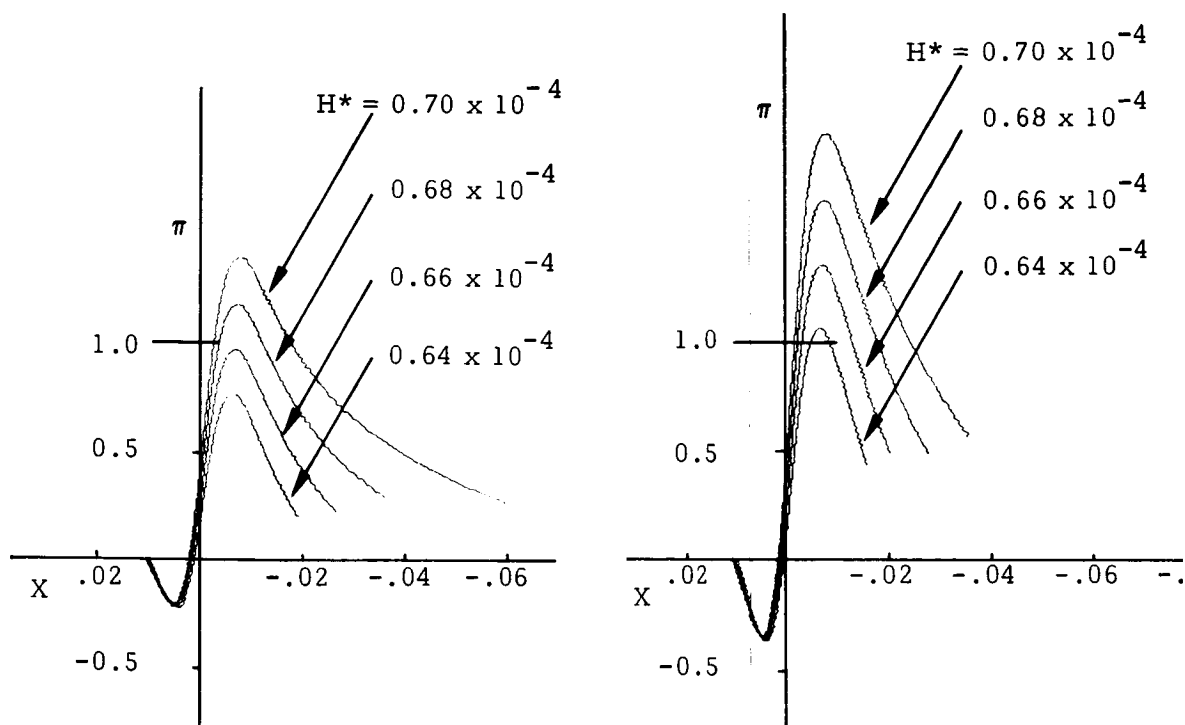
H^*	L	H_∞	Δ
0.070×10^{-3}	0.0423	0.1092×10^{-3}	0.0742×10^{-3}
0.068×10^{-3}	0.0281	0.0733×10^{-3}	0.0393×10^{-3}
0.066×10^{-3}	0.0192	0.0483×10^{-3}	0.0153×10^{-3}
0.064×10^{-3}	0.0099	0.0378×10^{-3}	0.0058×10^{-3}

Fig. 6.2.3
Pressure Distribution in Quasi
Two-Dimensional Flow Under
Rigid Circular Tire

$$H_O = 0.5 \times 10^{-4}$$
$$C = 2.0$$
$$\epsilon = 2 \times 10^{-6}$$

L	H_∞	Δ
0.0418	0.2748×10^{-3}	0.2398×10^{-3}
0.0244	0.1110×10^{-3}	0.0770×10^{-3}
0.0150	0.0890×10^{-3}	0.0360×10^{-3}
0.0085	0.0445×10^{-3}	0.0125×10^{-3}

Fig. 6.2.2
Pressure Distribution in Quasi
Two-Dimensional Flow Under
Rigid Circular Tire

$$H_O = 0.5 \times 10^{-4}$$
$$C = 1.0$$
$$\epsilon = \sqrt{2} \times 10^{-6}$$

6.3   Quasi Two-Dimensional Flow Model with Side Flow Estimate

Coupled with a Rigid Circular Tire*

Equations

$$\frac{df}{dx} = -6\pi_c H^2 \left(\frac{r_o}{6}\right)^2 \frac{1}{\epsilon} + \frac{3+f}{H}\frac{dH}{dx}$$

(6.3.1)

$$\frac{d\pi_c}{dx} = -\frac{\epsilon}{3H^2}f + \frac{C}{30H}(f-5)\frac{dH}{dx} - \frac{C}{15}\left(f+\frac{5}{2}\right)\frac{df}{dx}$$

(6.3.2)

$$H = H_o + \frac{x^2}{2}$$

(6.3.3)*

Input Parameters

ϵ, C, B, H_o, X_e

Boundary Conditions (integration in the negative x-direction)

At the exit:

$X = X_e$

$f_e = -1$

$\pi_e = 0$

(H_e is found from Eq. (6.3.3)).

At the inlet: The intersection of the solution of Eq. (6.3.1) through Eq. (6.3.3) and Eq. (3.2.0) provides the inlet condition.

---

*The technique applies to an arbitrary shape.

Output Parameters

H_∞ (from Eq. (3.2.8)), Δ (from Eq. (3.2.7)), L (from Eq. (5.3.1)).

In this inverse solution we prescribe the film terminal point (X_e) as well as the tire center level (H_o) and we find as output the water level (H_∞), the jet thickness Δ and the load (L). Trial and error is eliminated in this way.

Results

Sample solutions are given in Figs. 6.3.1 through 6.3.4. In each of the figures, a single effect is studied. For each case, three curves are given: π, f and H/H_e versus X.

In the specific case studied in Fig. 6.3.1 the effect of reducing width is unoticeable until b/r_o is of the order of about 0.05. For lower values, however, the solution is affected. In fact, for $b/r_o = 0.025$ the "solution" presented in Fig. 6.3.1 – c does not meet the initial conditions. This is interpreted to mean that for small enough width no hydroplaning occurs. This phenomenon could be intuitively expected and here it is calculated quantitatively for the model considered.

Figure 6.3.2 exhibits the effect of changing the gap. Reduced gap means higher pressure and load. Figure 6.3.3 demonstrates the effect of changing X_e (the film separation point). The resulting pressure distribution is affected quite strongly by small variations of X_e.

The conclusion, with respect to the effect of speed, is that as the pressure level increases, the depth of penetration of the inlet point into the footprint area increases at the same time.

6.3.1-a

ϵ = 10^{-6}

C = 0.5

B = 1/3

H_o = 0.05 x 10^{-3}

X_e = 0.01

L = 0.131

H_∞ = 7.415 x 10^{-5}

Δ = 3.977 x 10^{-5}

6.3.1-b

ϵ = 10^{-6}

C = 0.5

B = 1/20

H_o = 0.05 x 10^{-3}

X_e = 0.01

L = 0.0149

H_∞ = 1.784 x 10^{-4}

Δ = 1.765 x 10^{-6}

6.3.1-c

ϵ = 10^{-6}

C = 0.5

B = 1/40

H_o = 0.05 x 10^{-3}

X_e = 0.01

Solution does not
meet inlet conditions.

Fig. 6.3.1 Pressure, Shape Factor, and Gap Distribution
in a Quasi Two-Dimensional Flow Model with
Side Flow Estimate Coupled with Rigid Circular
Tire; Effect of Width Parameter B

6.3.2-a

ϵ = 10^{-6}

C = 0.5

B = 1/3
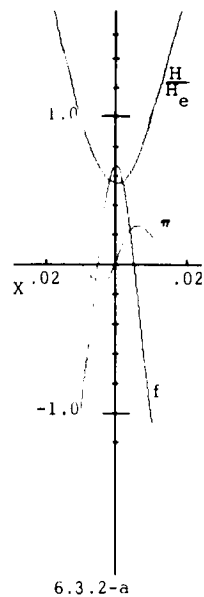
H_o = 0.06×10^{-3}

X_e = 0.01

L = 0.0013

H_∞ = 3.668×10^{-5}

Δ = 3.704×10^{-9}

6.3.2-b

ϵ = 10^{-6}

C = 0.5

B = 1/3
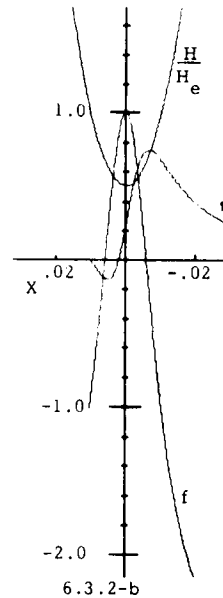
H_o = 0.05×10^{-3}

X_e = 0.01

L = 0.0131

H_∞ = 7.415×10^{-5}

Δ = 3.977×10^{-5}

Fig 6.3.2 Pressure, Shape Factor, and Gap Distribution in a Quasi Two-Dimensional Flow Model with Side Flow Estimate Coupled with Rigid Circular Tire; Effect of H_o

6.3.3-a

ϵ = 10^{-6}
C = 0.5
B = 1/3
H_o = 0.05 x 10^{-3}
X_e = 0.009
L = 0.0012
H_∞ = 3.017 x 10^{-5}
Δ = 0.00

6.3.3-b

ϵ = 10^{-6}
C = 0.5
B = 1/3
H_o = 0.05 x 10^{-3}
X_e - 0.01
L = 0.0131
H_∞ = 7.415 x 10^{-5}
Δ = 3.977 x 10^{-5}

6.3.3-c

ϵ = 10^{-6}
C = 0.5
B = 1/3
H_o = 0.05 x 10^{-3}
X_e = 0.0105
L = 0.0397
H_∞ = 9.435 x 10^{-4}
Δ = 2.498 x 10^{-6}
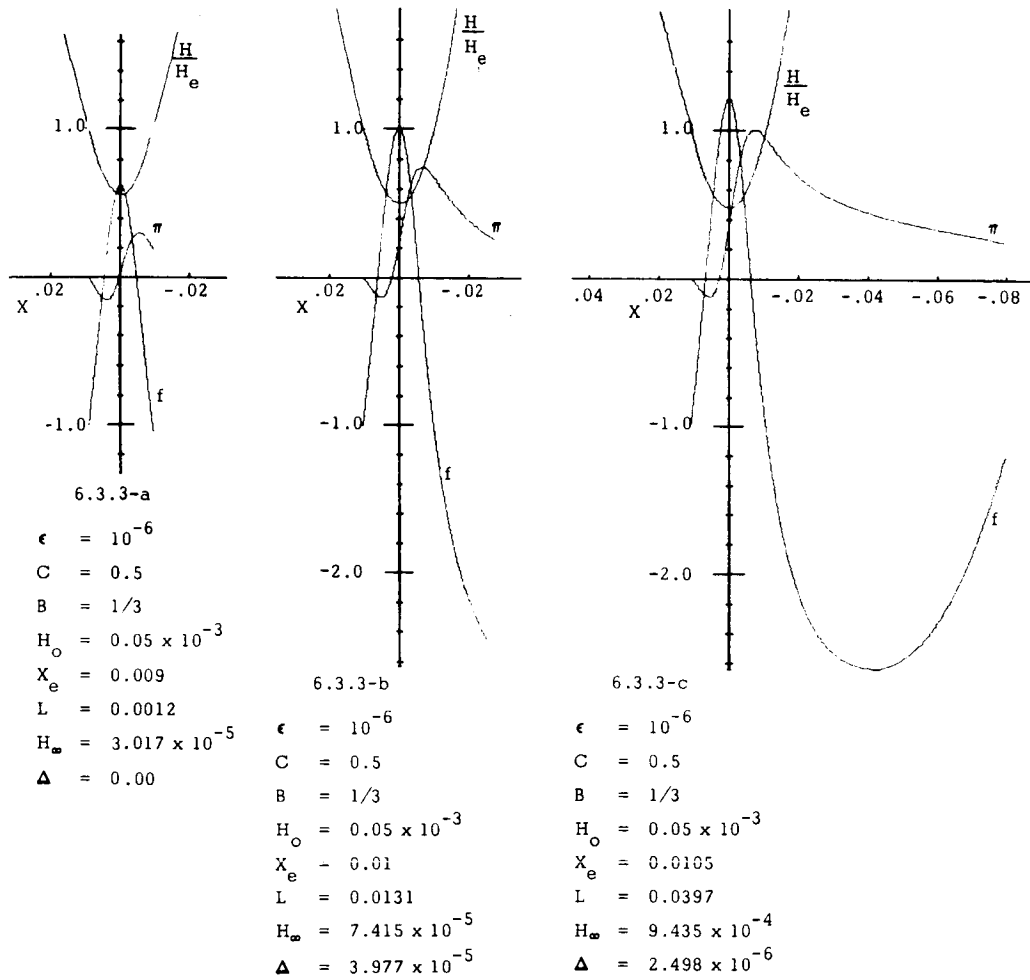
Fig. 6.3.3   Pressure, Shape Factor, and Gap Distribution
in a Quasi Two-Dimensional Flow Model
with Side Flow Estimate Coupled with Rigid
Circular Tire; Effect of X_e

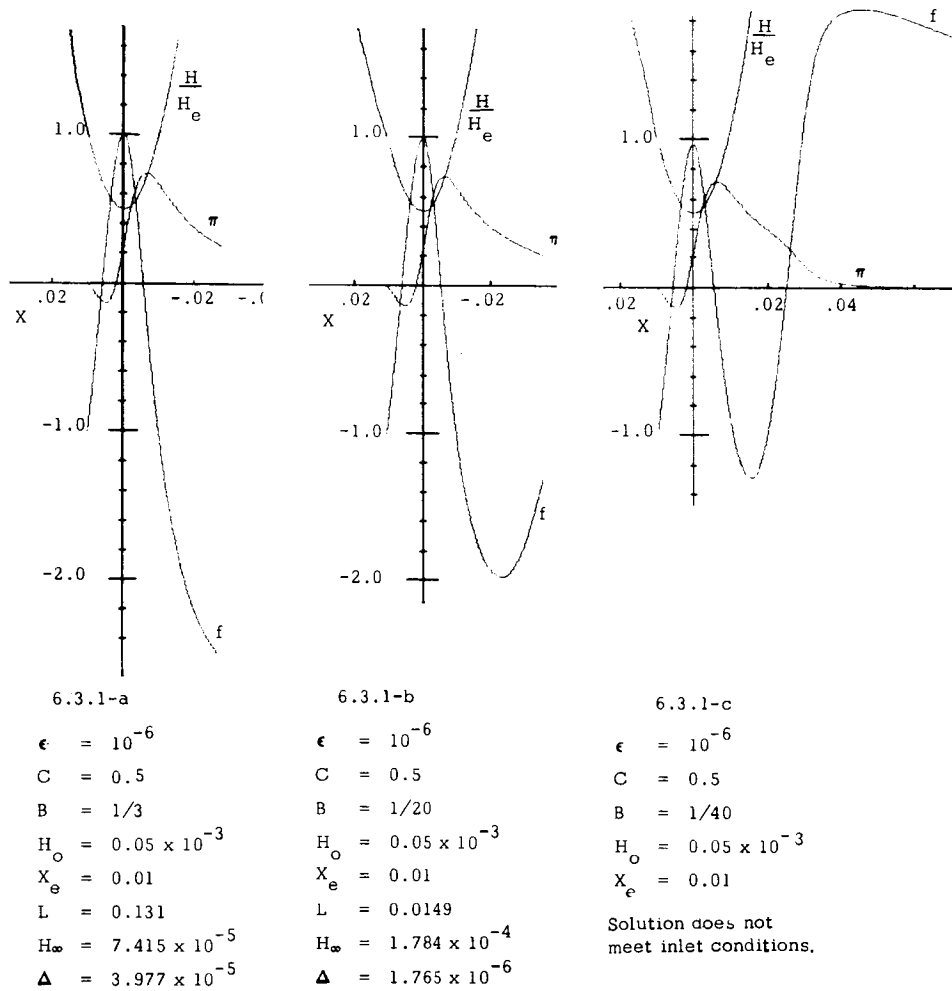| 6.3.4-a	6.3.4-b	6.3.4-c	6.3.4-d
$\epsilon = 0.707 \times 10^{-6}$	$\epsilon = 10^{-6}$	$\epsilon = 1.414 \times 10^{-6}$	$\epsilon = 2.0 \times 10^{-6}$
$C = 0.25$	$C = 0.5$	$C = 1.0$	$C = 2.0$
$B = 1/3$	$B = 1/3$	$B = 1/3$	$B = 1/3$
$H_o = 0.05 \times 10^{-3}$	$H_o = 0.5$	$H_o = 0.05 \times 10^{-3}$	$H_o = 0.05 \times 10^{-3}$
$X_e = 0.01$	$X_e = 0.01$	$X_e = 0.01$	$X_e = 0.01$
$L = 0.0119$	$L = 0.0131$	$L = 0.0147$	$L = 0.0168$
$H_\infty = 1.408 \times 10^{-4}$	$H_\infty = 7.415 \times 10^{-5}$	$H_\infty = 4.941 \times 10^{-5}$	$H_\infty = 4.063 \times 10^{-5}$
$\Delta = 9.879 \times 10^{-5}$	$\Delta = 3.977 \times 10^{-5}$	$\Delta = 1.583 \times 10^{-5}$	$\Delta = 7.182 \times 10^{-6}$
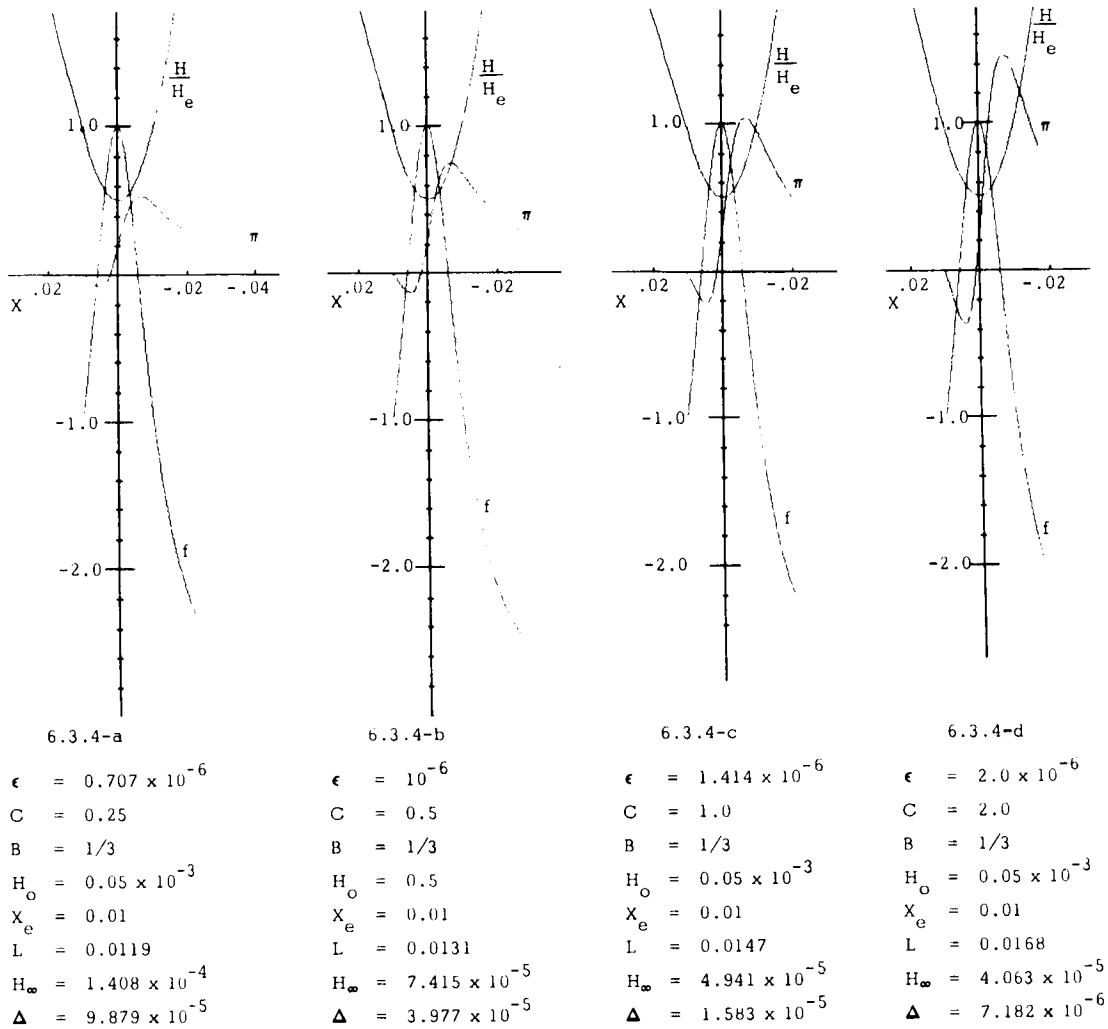
Fig. 6.3.4 Pressure, Shape Factor, and Gap Distribution
in a Quasi Two-Dimensional Flow Model with
Side Flow Estimate Coupled with Rigid Circular
Tire; Effect of Speed ($\epsilon \sim U$; $C \sim U^2$)

6.4   Foil Bearing (Quasi Two-Dimensional Flow Coupled with a
        Perfectly Flexible Foil Tire Model)

Equations: (See Section 2.2, 5.5)

$$\frac{d\pi}{dx} = -\frac{\epsilon}{H^2}\left(\frac{H^*}{H} - 1\right) + \frac{C}{15}\frac{dH}{dx}\left(\frac{9H^{*2}}{H^3} - \frac{4}{H}\right) \tag{6.4.1}$$

$$f = 3\frac{H^*}{H} - 3 \tag{6.4.2}$$

$$\frac{d^2H}{dx^2} = 1 - \pi \tag{6.4.3}$$

Input Parameters

ϵ, C, H*, H'_e

Boundary conditions

At the exit:

$$\pi_e = 0$$

$$f = -1$$

$$\frac{dH}{dx_e} = H'_e$$

(H_e and H''_e are found from Eq. (6.4.2) and (6.4.3)).

The numerical integration of Eqs. (6.4.1) and (6.4.3) gives a relation between π and H.

At the inlet:

At the inlet: Eq. (3. 2. 9) supplies a second relation between π and H so that the inlet point is determined.

Output Parameters

H_∞ (from Eq. 3. 2. 8)), No Load.

Results

We have described above the formulation of the foil bearing problem, using notation and approach consistent with the rest of this report. In our preliminary work we have used a somewhat different formulation and notation. At that time, the initial conditions, Eqs. (3. 2. 7) through (3. 2. 9) had not yet been derived and only the case, C = 0, was calculated. Due to the limited applicability of the foil bearing model (no hub load transmission), it has not been pursued any further and is presented in Fig. 6. 4. 1 in the original form. The notation used in Fig. 6. 4. 1 differs from that of this work. It is defined in the left hand side of the following relations in terms of our present notation

$$H \longleftarrow \frac{h}{r_0} \epsilon^{-2/3} \tag{6. 4. 4}$$

$$H^* \longleftarrow \frac{h^*}{r_0} \epsilon^{-2/3} \tag{6. 4. 5}$$

$$\bar{H} \longleftarrow \frac{h}{h^*} \tag{6. 4. 6}$$

$$\xi \leftarrow \frac{x}{r_o} \epsilon^{-1/3} \tag{6.4.7}$$

$$\bar{\xi} \leftarrow \frac{x}{\rho_*} \epsilon^{1/3} \tag{6.4.8}$$

Fig. 6.4.1 was originally designed to be used with prescribed pressure π_i and clearance H_i according to the following recipe.

(a) $$H_i'' = 1 - \pi_i$$

(b) $$\bar{H}_i'' \bar{H}_i = H_i'' H_i$$

(c) With the value of $\bar{H}_i'' \bar{H}_i$ find from Fig. 6.4.1 the values of

$$\bar{\xi}_i \quad , \quad \bar{H}_i \quad , \quad \bar{H}_i''$$

(d) $$H^* = \frac{H_i}{\bar{H}_i}$$

(e) Choose the corresponding exit region curve.

$\bar{H} = \dfrac{H}{H^*}$

14

12

10

8

6

4

2

0

$\bar{H}''\ \ \bar{H} = H''\,H$

8

6

4

2

0

$\bar{H}'' = H''H^*$

0.6

0.4

0.2

0

73
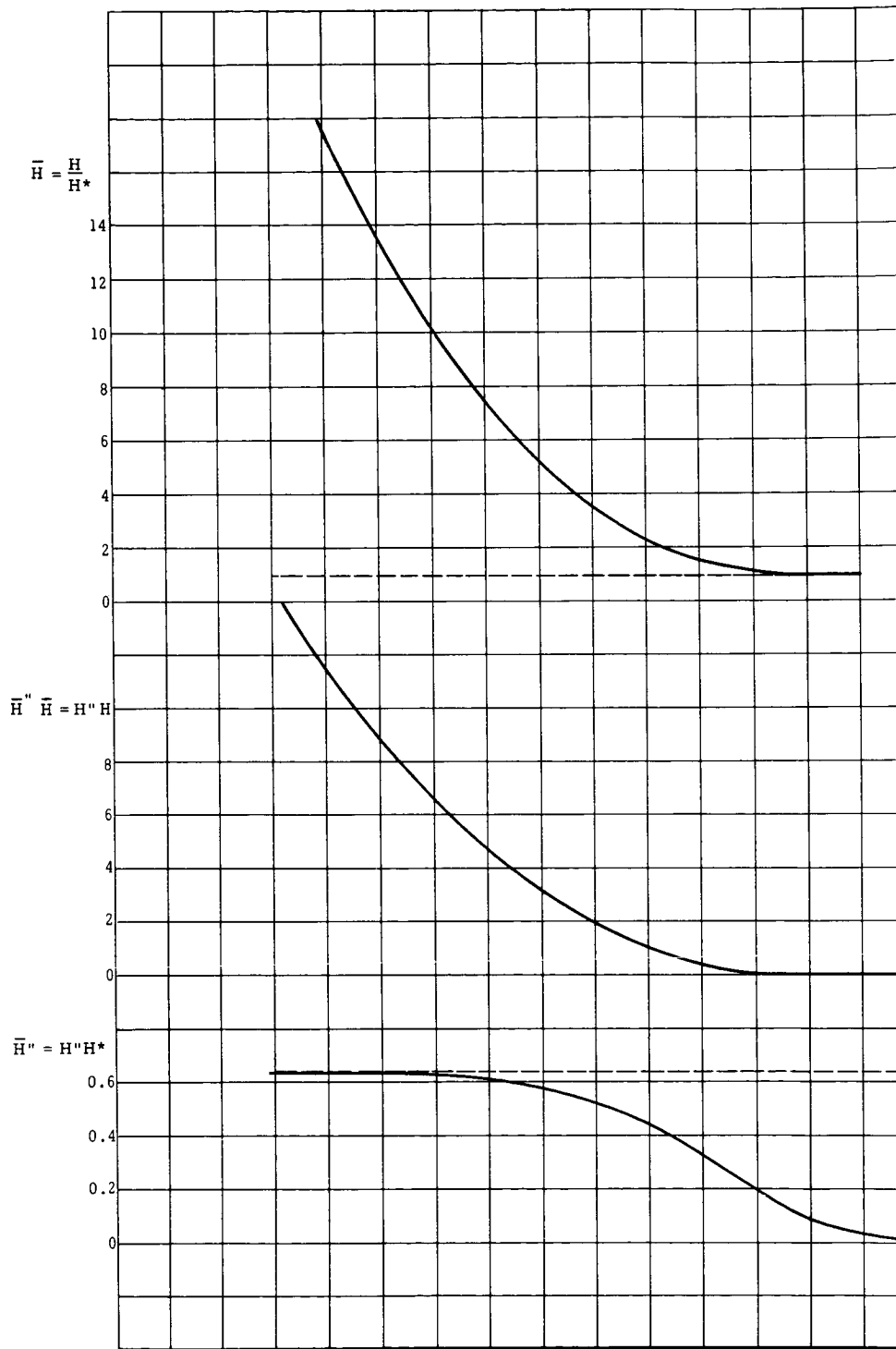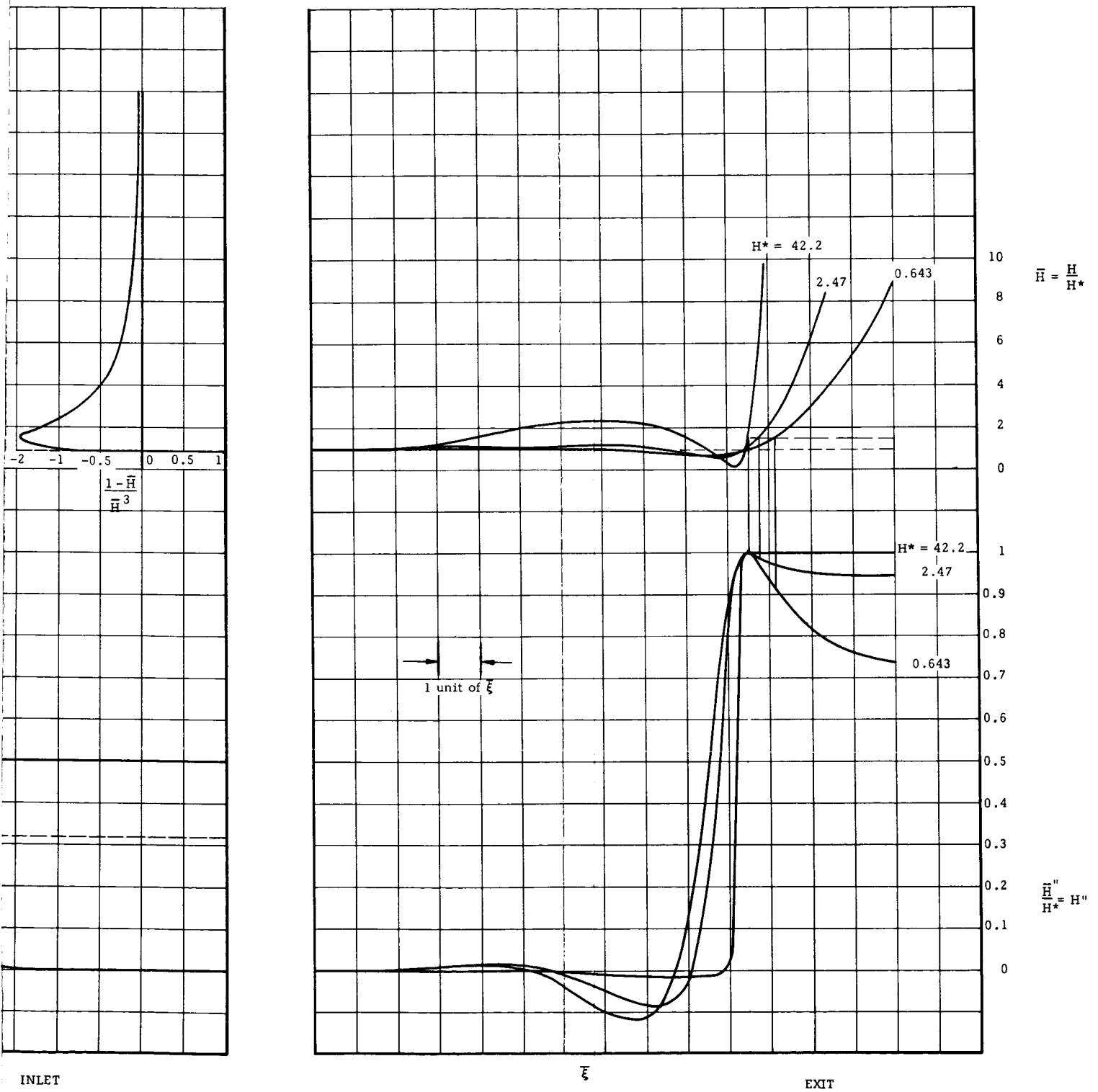
Fig. 6.4.1 The Film Thickness Distribution and Its Derivatives
for the Foil Bearing Model with C = 0

6.5 Quasi Two-Dimensional Flow Coupled with Tire-Spring Model

Equations (See Section 2.2; 5.6.)

$$\frac{d\pi}{dx} = -\frac{\epsilon}{H^2}\left(\frac{H^*}{H} - 1\right) + \frac{C}{15}\frac{dH}{dx}\left(\frac{9H^*}{H^3} - \frac{4}{H}\right) \tag{6.5.1}$$

$$f = 3\frac{H^*}{H} - 3 \tag{6.5.2}$$

$$W = \frac{1}{K_W}\left(1 - \pi\right) \tag{6.5.3}$$

$$H = H_o + \frac{X^2}{2} - W \tag{6.5.4}$$

Input Parameters

ϵ, C, H*, K_W, H_o (note $W_o = \dfrac{1}{K_W}$).

Boundary Conditions (integrating in the negative x-direction).

At the Exit:

$$\pi_e = 0 \tag{6.5.5}$$

$$f_e = -1 \tag{6.5.6}$$

From Eqs. (6.5.3) and (6.5.5) it follows that

$$W_e = \frac{1}{K_W} \tag{6.5.7}$$

The value of H_e can be found from Eq. (6.5.2). Finally, the value of X_e can then be found from Eq. (6.5.4).

At the inlet: The intersection of the solution of Eq. (6.5.1) and of Eq. (3.2.9) determines the inlet point.

Output Parameters

H_∞ (from Eq. 3.2.8), L, and M.

Results

In Fig. 6. 5. 1, typical results for the spring model are shown. The distributions of pressure shape factor, deflection and relative gap size are shown. It is seen that for small values of W_O (nearly rigid tire), the results are not qualitatively different from those for a rigid tire. When W_O is increased, the pressure distribution shows spikes. This can be explained by the fact that the model consists of independent springs. Sharp pressure variations will cause sharp gap variations. The exit sub-atmospheric pressure causes a local reduction of gap and restricts the flow. This affects the whole pressure distribution. Had the springs been inter-dependent, a local sharp variation in pressure would more smoothly distribute its effect on the deflection. It is concluded, therefore, that a more elaborate elastic model is needed to describe hydroplaning even qualitatively.

6. 6   Quasi Two-Dimensional Flow Coupled with the Tire - Membrane Model

Equations (See Section 2. 2; 5. 8.)

$$\frac{d\pi}{dx} = -\frac{\epsilon}{H^2}\left(\frac{H^*}{H} - 1\right) + \frac{C}{15}\frac{dH}{dx}\left(\frac{9H^*}{H^3} - \frac{4}{H}\right) \qquad (6.6.1)$$

$$f = 3\frac{H^*}{H} - 3 \qquad (6.6.2)$$

$$\frac{d^2H}{dx^2} = \frac{1}{K_T} - \frac{\pi}{K_T} + \frac{K_W}{K_T}H - \frac{K_W}{K_T}\left(H_O + \frac{x^2}{2}\right) \qquad (6.6.3)$$

$H^* = 0.07 \times 10^{-3}$
$H_o = 0.05 \times 10^{-3}$
$C = 0.5$
$\epsilon = 10^{-6}$

W_o	L	H_∞	Δ
0	0.04510	0.944×10^{-3}	0.909×10^{-3}
5×10^{-5}	0.09029	1.586×10^{-3}	1.551×10^{-3}
10×10^{-5}	0.05875	4.678×10^{-4}	4.328×10^{-4}

$W_o = 0$
6.5.1-a

$W_o = 5 \times 10^{-5}$
6.5.1-b

$W_o = 10 \times 10^{-5}$
6.5.1-c

Fig. 6.5.1 Pressure, Gap, and Deflection Distribution in a Quasi Two-Dimensional Flow Coupled with the Tire Spring Model

Input Parameters

$$\epsilon, \ C, \ H^*, \ K_T, \ K_W, \ H_o$$

Boundary Conditions (integrating in the negative x-direction)

At the exit:

$$X_e = \text{Trial Value}$$

$$\pi_e = 0 \tag{6.6.4}$$

$$f_e = -1 \tag{6.6.5}$$

$$H_e' = -\sqrt{\frac{K_W}{K_T}} \left(H_e - H_o - \frac{X_e^2}{2} - \frac{K_T - 1}{K_W} \right) + X_e \tag{6.6.6}$$

H_e is found from Eqs. (6.6.5) and (6.6.2). H_e'' is found from Eqs. (6.6.4) and 6.6.3).

At the inlet: The intersection of the solution of Eqs. (6.6.1) through (6.6.3) and Eq. (3.2.9) provides the inlet condition. The slope continuity requirement for the inlet region must also be satisfied, i. e.,

$$H_i' = \sqrt{\frac{K_W}{K_T}} \left(H_i - H_o - \frac{X_i^2}{2} - \frac{K_T - 1}{K_W} \right) + X_i$$

This requirement may be used to determine the correct value of X_e by trial and error.

Output Parameters:

H_∞ (from Eq. (3. 2. 8)), L, and M.

Results

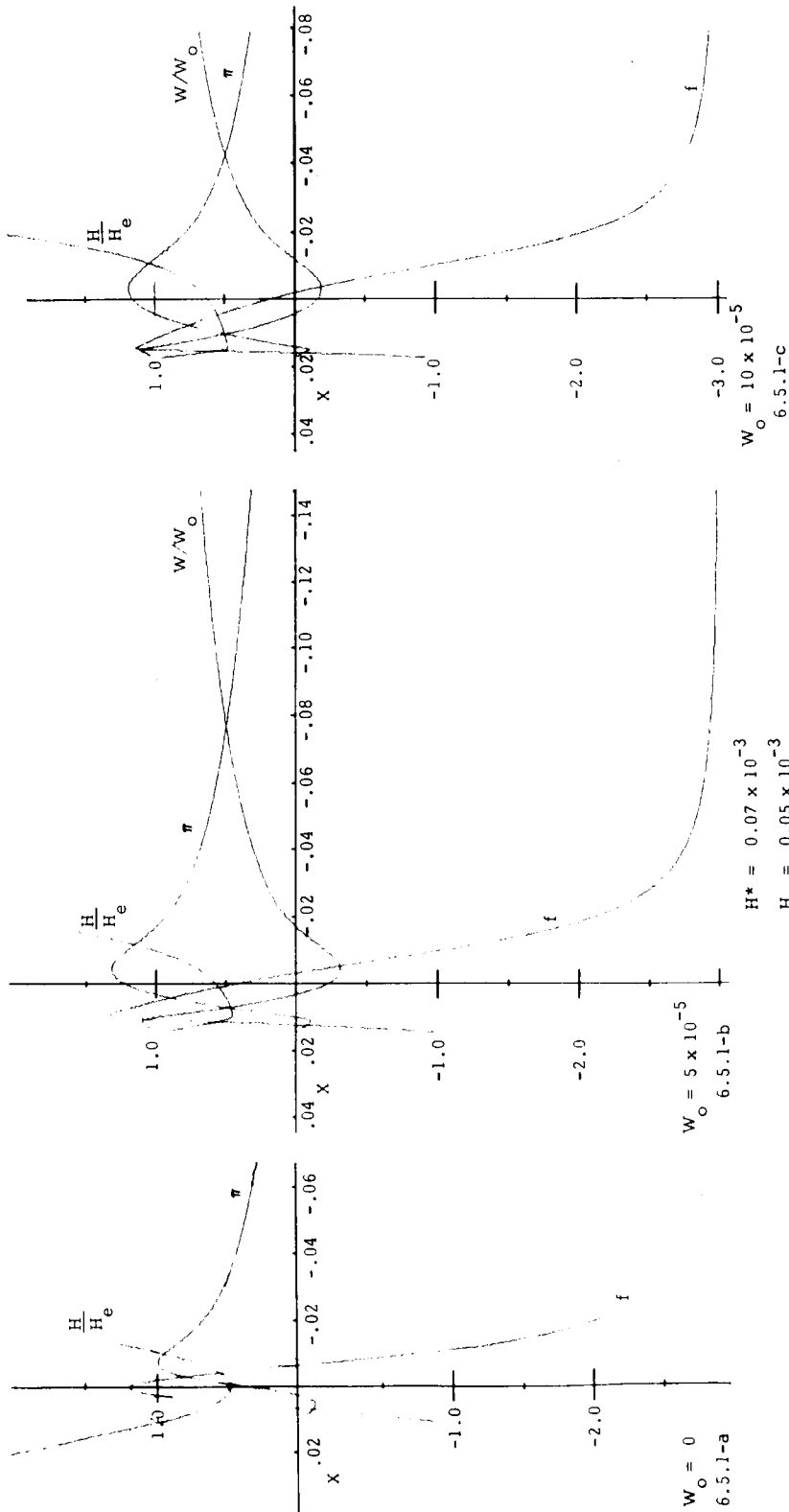The above formulation has been programed for numerical solution but results have not yet been obtained.

6.7 Quasi Two-Dimensional Flow Coupled with the Tire Shell Model.

Equations (See Section 2. 2; 5. 7.)

$$\frac{d\pi}{dx} = -\frac{\epsilon}{H^2}\left(\frac{H^*}{H} - 1\right) + \frac{C}{15}\frac{dH}{dx}\left(\frac{9H^*}{H^3} - \frac{4}{H}\right) \qquad (6.7.1)$$

$$f = 3\frac{H^*}{H} - 3 \qquad (6.7.2)$$

$$H = H_0 + \frac{x^2}{2} + \frac{K_T - 1}{K_W} + \int_{X_i}^{X_e} \pi(\xi)\, G(x,\xi)\, d\xi \qquad (6.7.3)$$

where $G(x, \xi)$ is defined in Eq (5. 7. 43) and depends on the parameters K_T, K_W, K_D.

Input Parameters

$$\epsilon, \ C, \ H^*, \ K_T, \ K_W, \ K_D, \ H_o$$

Boundary Conditions and Procedure

Assume $H = H_1(x)$ (trial distribution). At the exit:

$$\pi_e = 0$$

$$f_e = -1.$$

The value of H_e is found from Eq. (6.7.2) and the corresponding value of X_e from the trial distribution. Integration of Eq (6.7.1) supplies a relation between π and H. The attachment point $(\pi_i, \ H_i)$ must belong to this family.

At the inlet: Eq. (3.2.9) supplies a second relation between π_i and H_i so that the inlet point X_i is determined.

Now then, Eq. (6.7.3) can be integrated to produce a new corrected gap distribution $H = H_2(x)$ and thus the process may be repeated until input distribution $H_k(x)$ differs from the output distribution $H_{k+1}(x)$ by no more than a prescribed error. Techniques for facilitating convergence will probably have to be used.

Output Parameters

H_∞ (from Eq. 3. 2. 8), L and M (Eqs. (5. 3. 1, 5. 3. 2))

The iterative process described above has been programmed and considerable segments of the program have been debugged. Results have not yet been obtained.

6. 8 Quasi Three-Dimensional Flow Coupled with a Rigid Cylindrical Tire

Equations (See Section 2. 1; 5. 4.)

$$\left(f + \frac{5}{2}\right)\frac{\partial f}{\partial x} + g\frac{\partial f}{\partial z} + \frac{15}{C}\frac{\partial \pi}{\partial x} = -\frac{5\epsilon}{CH^2}f + \frac{f-5}{2H}\frac{dH}{dx} \qquad (6.8.1)$$

$$\left(f + \frac{5}{2}\right)\frac{\partial g}{\partial x} + g\frac{\partial g}{\partial z} + \frac{15}{C}\frac{\partial \pi}{\partial z} = -\frac{5\epsilon}{CH^2}g + \frac{g}{2H}\frac{dH}{dx} \qquad (6.8.2)$$

$$\frac{\partial f}{\partial x} + \frac{\partial g}{\partial z} = -\frac{3+f}{H}\frac{dH}{dx} \qquad (6.8.3)$$

$$H = H_o + \frac{x^2}{2} \qquad (6.8.4)$$

This is a rather complicated set of nonlinear partial differential equations. The first question which one faces in attempting to devise a solution technique is the type of the equations. This may be answered by finding the lines along which discontinuities in the solution propagate, namely the characteristics.

82

Given f, g, π along a line of slope dX/dZ passing at a point X, Z, what are the partial derivatives $\frac{\partial f}{\partial x}$, $\frac{\partial f}{\partial z}$ at the point? To answer this question, we write Eqs. (6. 8. 1) to (6. 8. 3) and the expressions for the differentials df, dg, dπ in the matrix form

$$
\begin{bmatrix}
f+\frac{5}{2} & g & 0 & 0 & \frac{15}{c} & 0 \\
0 & 0 & f+\frac{5}{2} & g & 0 & \frac{15}{c} \\
1 & 0 & 0 & 1 & 0 & 0 \\
dx & dz & 0 & 0 & 0 & 0 \\
0 & 0 & dx & dz & 0 & 0 \\
0 & 0 & 0 & 0 & dx & dz
\end{bmatrix}
\cdot
\begin{bmatrix}
\frac{\partial f}{\partial x} \\
\frac{\partial f}{\partial z} \\
\frac{\partial g}{\partial x} \\
\frac{\partial g}{\partial z} \\
\frac{\partial \pi}{\partial x} \\
\frac{\partial \pi}{\partial z}
\end{bmatrix}
=
\begin{bmatrix}
-\frac{5\epsilon}{cH^2}f + \frac{f-5}{2H}\frac{dH}{dx} \\
-\frac{5\epsilon}{cH^2}g + \frac{g}{2H}\frac{dH}{dx} \\
-\frac{3+f}{H}\frac{dH}{dx} \\
df \\
dg \\
d\pi
\end{bmatrix}
$$

A unique solution for the derivatives exists only if the determinant of the coefficients does not vanish. For those lines of slope, dX/dZ, if any, in which the determinant vanishes, the derivatives are non-unique and discontinuities in the derivatives across the line may occur. In our case, the determinant of the coefficients vanishes along the characteristic curve whose local slope is:

$$\frac{dx}{dz} = \frac{f + 5/2}{g} \tag{6.8.5}$$

Thus the equations have a single real characteristic and two imaginary ones. The third order system is thus partly an initial value problem and partly a boundary value problem.

By moving the pressure derivatives to the right-hand side and pairing the first and fourth equation and the second and fifth equation in the matrix, it may be seen that along the characteristic curve

$$\left(\frac{df}{dx}\right)_{Char} = \frac{-\frac{5\epsilon}{C H^2} f + \frac{f-5}{2H}\frac{dH}{dx} - \frac{15}{C}\frac{\partial \pi}{\partial x}}{f + \frac{5}{2}} \tag{6.8.6}$$

$$\left(\frac{dg}{dx}\right)_{Char} = \frac{-\frac{5\epsilon}{C H^2} g + \frac{g}{2H}\frac{dH}{dx} - \frac{15}{C}\frac{\partial \pi}{\partial z}}{f + \frac{5}{2}} \tag{6.8.7}$$

We can conclude that for a given π (X, Z), it is sufficient to know f and g at a point in order to find f and g along the characteristic curve passing through that point. This exhibits the initial-value problem character of the equations.

On the other hand, by differentiating Eq. (6.8.1) and (6.8.2) with respect to X and Z respectively, adding and using Eq. (6.8.3) we find.

$$\nabla^2 \pi = \left[\left(f + \frac{\xi}{2}\right) \frac{\partial}{\partial x} + g \frac{\partial}{\partial z} + \frac{5\epsilon}{CH^2} - \frac{1}{2H} \frac{d \ln H}{dx} \right]\left(\frac{3+f}{H} \frac{dH}{dx}\right) +$$

$$+ \frac{10\epsilon}{CH^3} \frac{dH}{dx} f + \frac{f - \sigma}{2} \frac{d^2 \ln H}{dx^2} - \left(\frac{\partial f}{\partial x}\right)^2 - \left(\frac{\partial g}{\partial z}\right)^2 - 2\frac{\partial g}{\partial x} \frac{\partial f}{\partial z} \qquad (6.8.8)$$

This is a Poisson's equation and can be solved for a given f(X, Z), g(X, Z) and a prescribed π on the boundary. This exhibits the boundary-value-problem character of the equations.

Thus we have a basis for an iterative procedure: Given π – find f and g. Given f and g, find π. It should be stressed that the problem has not been well set in the above in terms of boundary conditions. We will only say that we have attempted a number of solutions by supplementing the above procedure with additional conditions. Details are not reported here since results have not been obtained.

One of the approaches which were studied resulted in the following analysis which is of some interest. Consider a flat plate of finite width and length moving over a layer of fluid of uniform height h. Side flow is allowed.

Eqs. (2. 1. 13)through (2. 1. 15) become:

$$\left(f + \frac{5}{2}\right)\frac{\partial f}{\partial x} + g\frac{\partial f}{\partial z} + \frac{30}{\rho U^2}\frac{\partial p}{\partial x} = -\frac{60\mu U}{\rho U^2 h^2}f \tag{6.8.9}$$

$$\left(f + \frac{5}{2}\right)\frac{\partial g}{\partial x} + g\frac{\partial g}{\partial z} + \frac{30}{\rho U^2}\frac{\partial p}{\partial z} = -\frac{60\mu U}{\rho U^2 h^2}f \tag{6.8.10}$$

$$\frac{\partial f}{\partial x} + \frac{\partial g}{\partial z} = 0 \tag{6.8.11}$$

The boundary conditions are $p = p_a$ on the boundaries and f prescribed on those sections of the boundary where the flow enters. If f = 0 is prescribed at the entrance (corresponding to Couette flow), the solution of the above system is $p \equiv p_a$; $f \equiv 0$; $g \equiv 0$.

Suppose, now, that the flow at the entrance is prescribed by some $f = f_0$ where $f_0 \ll 2.5$. The equation may be linearized as follows:

$$\frac{5}{2}\frac{\partial f}{\partial x} + \frac{30}{\rho U^2}\frac{\partial p}{\partial x} = -\frac{60\mu U}{\rho U^2 h^2}f \tag{6.8.12}$$

$$\frac{5}{2}\frac{\partial g}{\partial x} + \frac{30}{\rho U^2}\frac{\partial p}{\partial z} = -\frac{60\mu U}{\rho U^2 h^2}g \tag{6.8.13}$$

$$\frac{\partial f}{\partial x} + \frac{\partial g}{\partial z} = 0 \tag{6.8.14}$$

The solution is:

$$p = p_a \tag{6.8.15}$$

$$f = f_0 \, e^{-\frac{24 \mu U}{\rho U^2 h^2} x} \tag{6.8.16}$$

$$g = f_0 \, z \, e^{-\frac{24 \mu U}{\rho U^2 h^2} x} \tag{6.8.17}$$

This means that the flow tends to Couette flow in a transition layer of the order

$$\frac{x}{h} \sim \frac{1}{24} \frac{\rho U h}{\mu} \tag{6.8.18}$$

6.9   Quasi Two-Dimensional Non-Viscous Flow Model Coupled with the Spring Tire Model

Equations (See Section 2.4; 5.6)

$$\hat{u} \, H = H_\infty \qquad \text{(Continuity)} \tag{6.9.1}$$

$$C + \pi = 1 \qquad \text{(Bernoulli)} \tag{6.9.2}$$

$$H + W = H_o + X^2/2 \qquad \text{(Geometry)} \qquad (6.9\ 3)$$

$$1 - \pi = K_w W \qquad \text{(Elasticity)} \qquad (6.9.4)$$

Input Parameters

$$H_o \ , \quad K_W \ , \quad H_o$$

(Note: $W_o = 1/K_W$. W_o is a measure of the compliance of the tire.)

Solution

The pressure distribution $\pi = \pi(X)$ becomes:

$$\frac{X^2}{2} = W_o \left(1 - \pi\right) + \frac{H_\infty}{\left(1 - \frac{\pi}{C}\right)^{1/2}} - H_o \qquad (6.9.5)$$

In order for a solution to exist, the right hand side of this equation must go through zero. Otherwise, it would mean that no pressure exists corresponding to the tire center X = 0. X = 0 is a point of symmetry for the pressure distribution. By finding the minimum point of the right hand side of Eq. 6.9.5 and the condition for this minimum to be less than or equal to zero, we find that solution will exist only if

$$\frac{H_o}{H_{1\infty}} \geq \frac{W_o}{H_{1\infty}} \left(1 - C + \frac{C^{1/3}}{2^{2/3}} \left[\frac{H_{1\infty}}{W_o}\right]^{2/3}\right) + \frac{(2C)^{1/3}}{\left(\frac{H_{1\infty}}{W_o}\right)^{1/3}} \qquad (6.9.6)$$

This leads to the following interesting conclusions, which may be further understood from Fig. 6. 9. 1

When $W_o = 0$ (perfectly rigid tire); solutions alwasy exist.

When $W_o > 0$: If $C \leq 1$, solution can exist only for W_o less than some maximum value. On the other hand, if $C > 1$, there is a finite range of W_o for which no solution exists. For values higher than some threshold or lower than some threshold value, solutions exist. Physically, if $C < 1$, only convex tire shapes can exist. When flexibility is too high, the tire contacts the ground, and solutions do not exist. If $C > 1$, both concave and convex tire shapes can exist, depending on the degree of tire flexibility.

Some solution curves are shown in Fig 6. 9. 2. All the cases are at equal H_o, i. e. the tire center is at a fixed level and the fluid pressure may load it either up or down. The parameter which distinguishes the cases from one another is the degree of flexibility W_o.

In Fig. 6. 9. 2-a, the contour of a rigid tire ($W_o = 0$) is shown. In this case the pressure drops due to acceleration and reaches a minimum towards the center of the tire.

In Fig. 6. 9. 2-b a somewhat flexible tire is considered ($W_o = 0. 005$). It is seen that the pressure drops further close to the tire center.

When W_o is large enough, the pressure drops to such a low level that a "negative load" is locally produced and no solution according to our model is possible. This, however is only a hypothetical situation, since long before such an occurrence viscous effects will become important and the model discussed in this section will break down.
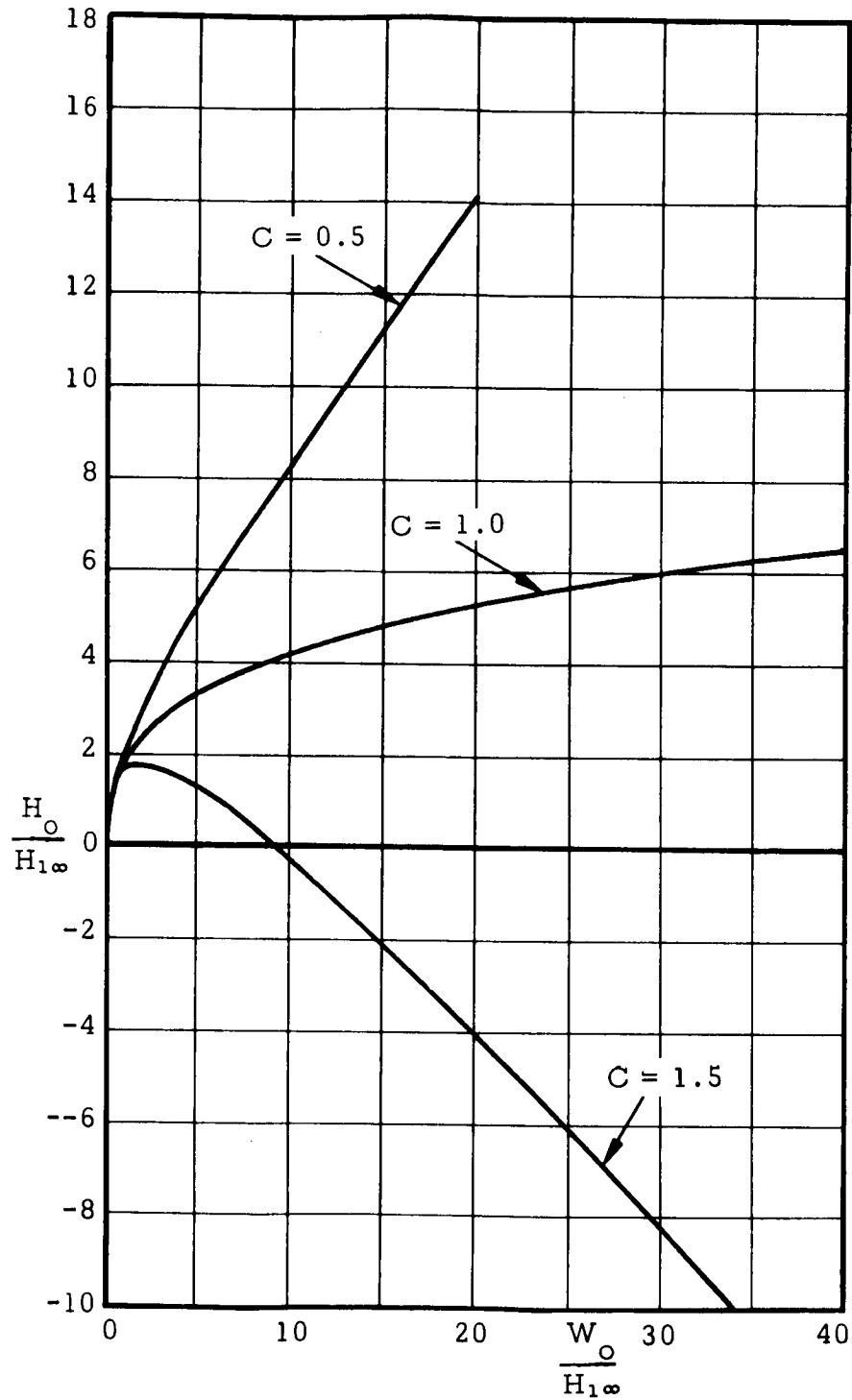
Fig. 6. 9. 1 Conditions for Existence of Solution for the Planar Friction
less Flow Approximation Coupled with the Tire Spring Model.
(Each curve separates the region above it, for which a solu-
tion exists, and the region below it, for which a solution does n
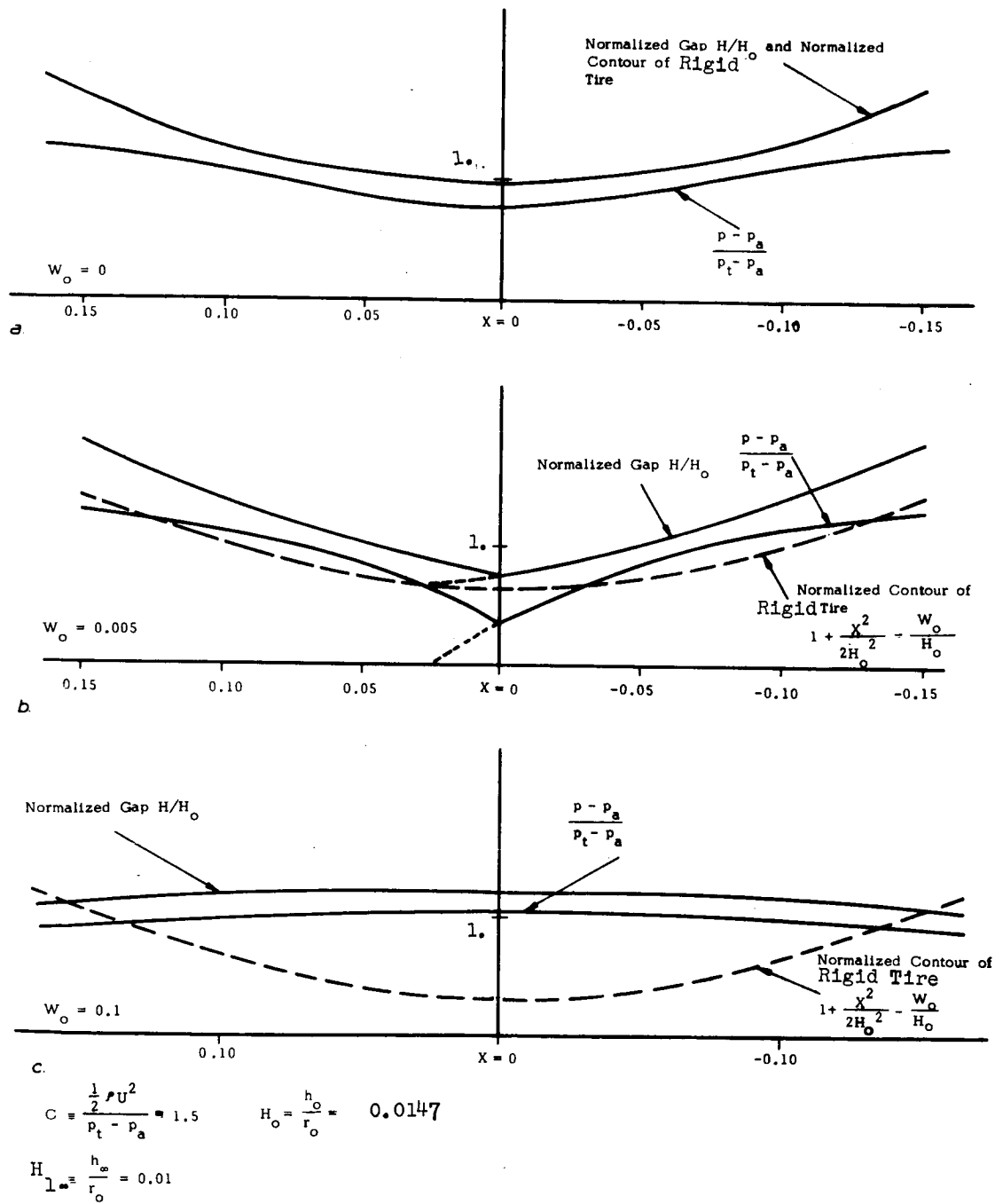not exist.)

Fig. 6.9.2 Typical Solutions for the Planar Frictionless Flow
Approximation Coupled with the Tire-Spring Model

Finally, Fig. 6.9.2-c shows a highly flexible tire in which, due to compliance, the film becomes divergent causing a peak of the pressure at the center, and further increase in load capacity. This is qualitatively the situation described by the NASA formula [9] which couples hydroplaning with flexibility.

7.0   REFERENCES

1.   Green, A. E., "Gliding on a Stream of Finite Depth, " Proc.
        Cambrdige Phil. Soc. 31, No. 4 (1935).

2.   Gurevich, M. I., "Theory of Jets in Ideal Fluids, " Academic
        Press, New York, 1965.

3.   Sedov, L. I., "Two-Dimensional Problems in Hydrodynamics
        and Aerodynamics, " Interscience Publishers, 1965.

4.   Martin, C. S., "Hydrodynamics of Tire Hydroplaning, " Final
        Report, Project B-608, Georgia Institute of Technology,
        1966.

5.   Birkhoff, G. and Zarantonello, E. H., "Jets, Wakes and
        Cavities, " Academic Press, New York, 1957.

6.   Kneschke, A., "Rollreibung auf spurbildender Fahrbahn, ",
        Ing. Arch., 25, 1957, 227-243.

7.   Birkhoff, G. and Hays, D. F., "Free Boundaries in Partial
        Lubrication, " J. Math. and Phys., 42, 2, 1963, 126-138.

8.   Coyne, J. C. and Elrod, H. G., Jr., "Conditions for the
        Rupture of a Lubricating Film, " Mechanical Technology Inc.,
        Report MTI-65TR58, 1965.

9.   Horne, W. B. and Dreher, R. C., "Phenomena of Pneumatic
        Tire Hydroplaning, " NASA TN-D-2058, Nov. 1963.

10.   Royal Aircraft Establishment, Mechanical Engineering Depart-
        ment, Farnborough, England - Film on Hydroplaning.

11.   Gross, W. A., Stahler, A., Wildmann, M., "A Comparison of
        the Characteristics of Self-Acting Foil Bearings and Pneumatic
        Tires, " Ampex Report RB 65-32, 1965.

RR 67-24

12. Eshel, A. and Elrod, H. G., Jr., "The Theory of the Infinitely Wide, Perfectly Flexible, Self-Acting Foil Bearing," ASME Trans., Vol. 87, Serv. D, Dec. 1965, 831-836.

13. Lauterbach, H. G. and Ames, W. F., "Cord Stresses in Inflated Tires," Textile Research J., Vol. 29, 1959.

14. Ames W. F., "Stresses in Cylindrically Symmetric Membranes Reinforced with Extensible Cords," J. Franklin Inst., 272, 3, 1961, 185-190.

15. Adkins, J. E., "Finite Plane Deformation of Thin Elastic Sheets Reinforced with Inextensible Cords," Phil. Trans. Roy. Soc., London, 1956, A249, 125-150.

16. J. E. Adkins, "Cylindrically Symmetrical Deformations of Incompressible Elastic Materials Reinforced with Inextensible Cords," J. Rat. Mech. and Anal., Vol. 5, 1956, 189-202.

17. Adkins, J. E. and Rivlin, "Large Elastic Deformations of Isotropic Material Reinforcement by Inextensible Cords," Roy. Soc. Phil. Trans., Vol. 248, 1955, 201-223.

18. Rivlin, R. S., "Plane Strain of a Net Formed by Inextensible Cords," J. of Rat. Mech. and Anal., 4, 1955, 951-974.

19. Hofferberth, D. W., "Zur Statik des Luftreifens," Kautschuk u. Gummi, Vol. 8, 1955, 124WT-BOWT.

20. Hofferberth, D. W., "Zur Festigkeit des Luftreifens," Kautschuk Gummi, Vol. 9, 1956, WT225-WT231.

21. Clark, S. K., Dodge, R. N., Tielking, J. T. and Herzog, B., "Deformation and Stresses in an Inflated Aircraft Tire," University of Michigan, ORA Project 05608, Report No. 1, Oct. 1963.

22. Clark, S. K., "The Rolling Tire Under Load," S. A. E. Paper 650493, presented Chicago, May 1965.

23.   Bergman, W., "Theoretical Prediction of the Effect of Traction on Cornering Force," S.A.E. Paper, presented Chicago, June 1960.

24.   Saito, Y., "A Study of Dynamic Steering Properties of Pneumatic Tyres," Inst. of Mech. Engrs., London Int'l Tech. Congress, Sept. 1962.

25.   Lippmann, S.A., "Structural Mechanisms of Tires Leading to the Development of Steering Forces," S.A.E. paper 794C, Automotive Engrg. Congress, Detroit, Mich. 1964.

26.   Blok, H. and Van Rossum, J.J., "The Foil Bearing - A New Departure in Hydrodynamic Lubrication," Lub. Engr., Vol. 9, No. 6, 1953.

27.   Horne, W.B. and Joyner, U.T., "Some Effects of Runway Slush and Water on the Operations of Airplanes with Particular Reference to Jet Transports," S.A.E. Trans., Vol. 70, 1962, 99-108.

AMPEX